

Fibrous structures on diamond and carbon surfaces formed by hydrogen plasma under direct-current bias and field electron-emission properties

Koji Kobashi, Takeshi Tachibana, Yoshihiro Yokota, Nobuyuki Kawakami, and Kazushi Hayashi

Frontier Carbon Technology Project/Japan Fine Ceramics Center, c/o Kobe Steel, Ltd., 1-5-5 Takatsuka-dai, Nishi-ku, Kobe 651-2271, Japan

Kazuhiro Yamamoto, Yoshinori Koga, and Shuzo Fujiwara

National Institute of Advanced Industrial Science and Technology, Tsukuba Central 5, 1-1-1 Higashi, Tsukuba 305-8565, Japan

Yasuhiro Gotoh, Hironori Nakahara, Hiroshi Tsuji, and Junzo Ishikawa

Department of Electronic Science and Engineering, Graduate School of Engineering, Kyoto University, Yoshida-Honmachi, Sakyo-ku, Kyoto 606-8501, Japan

Franz A. Köck and Robert J. Nemanich

Department of Physics, North Carolina State University, Raleigh, North Carolina 27695-8202

(Received 15 April 2002; accepted 24 October 2002)

Polycrystalline diamond films, single crystal bulk diamonds, and diamond powder were treated in microwave plasma of hydrogen at 1.6 torr under a negative direct-current bias of -150 to -300 V without metal catalyst. It was found that fibrous structures, uniformly elongated along the direction normal to the specimen surface, were formed on the diamond surfaces. Similar experiments for glasslike carbon resulted in conical structures with frizzy fibers at the tops. Transmission electron microscopy measurements indicated that the fibers formed on diamond consisted of randomly oriented diamond nanocrystals with diameters of less than 10 nm, while the conical structures formed on glasslike carbon consisted of graphite nanocrystals. Field emission measurements of the fibrous specimens exhibited better emission efficiency than untreated ones. The field emission electron microscopy of the fibrous glasslike carbon showed a presence of discrete electron emission sites at a density of approximately $10,000$ sites/cm².

I. INTRODUCTION

Formation of fibrous structures on material surfaces is of practical importance for such applications as field emission of electrons, where sharp tips are effective to reduce the threshold electric field,¹⁻³ and chemical electrodes, including chemical and biosensors,^{4,5} where large surface areas are preferable to achieve better performance. For diamond, a high density of needlelike structures is often formed by oxygen-plasma etching,⁶ where a presence of dislocations or unintentional impurity particles at the initial surface masks and prevents local etching of the diamond surface. It has been, however, found by Stoner *et al.*⁷ that diamond films deposited on Si substrates can also be etched by microwave plasma of hydrogen, if a negative direct current (dc) bias is applied to the specimen against a counter electrode placed above the plasma. The etching conditions were {gas pressure P , bias voltage V_b , microwave power P_m , specimen temperature T_s } = {15 torr, -250 V, 800 W, 450 °C}

(1 torr = 133.3 Pa), where a modified stainless-steel-type microwave plasma generator (ASTeX-type, Seki Technotron Corp., Tokyo, Japan) was used. In the experiment, the entire diamond film was etched down to the Si substrate with an estimated etching rate of ≥ 6 $\mu\text{m/h}$. Jiang *et al.*^{8,9} performed similar experiments using (100)-oriented polycrystalline diamond films under conditions of {23 torr, -150 V, 1000 W, 780 °C} using an ASTeX-type plasma generator. After a hydrogen plasma treatment for 20 h, the (100) faces of the diamond grains at the film surface grew laterally, and as a consequence, their areas increased from about 1 to about 4 μm^2 . The (100) faces were roughened by hydrogen plasma etching at a rate of about 0.05 $\mu\text{m/h}$. A cause of the lateral growth was attributed to a preferential redeposition of diamond on the sides of (100) faces, where the H⁺-ion damage is weak. Yamamoto *et al.*¹⁰ carried out hydrogen plasma etching of polycrystalline diamond films using electron-cyclotron resonance plasma of hydrogen for 2 h

under conditions of $\{(3.9\text{--}6.9) \times 10^{-4}$ torr, a self-bias, 500 W, room temperature (RT), i.e., no substrate heating}. In this experiment, dc bias was not intentionally applied to the specimen, but a negative self-bias of about 1.5 kV was assumed to be present. As a result, the diamond surface was converted to fibrous structures, where each fiber was 30 nm in diameter near the top end, and 200–300 nm in length. Material characterizations of the fibrous structures have not yet been done, but it was shown that the field emission of electrons from the fibrous specimen increased significantly: with an anode of 1.1 mm diameter that was 6 μm away from the specimen surface, the emission current was 24.5 mA/cm² at 126 V (the average field was 21 V/ μm), while for an *as-grown* diamond film it was only 0.1 mA/cm² at 1500 V (the average field was 250 V/ μm).

For carbon materials other than diamond, extensive studies of carbon nanotube (CNT), discovered by Iijima,¹¹ and nanosize carbon allotropes are ongoing for various applications such as vacuum electron emitters for flat-panel displays^{12,13} and vacuum fluorescent tubes,^{14,15} hydrogen storage,^{16–18} battery electrodes,¹⁹ and one-dimensional devices.^{20,21} For synthesis of CNTs, arc discharge, hydrocarbon pyrolysis, and laser ablation have been used. One can refer to recent reviews^{22,23} on these topics. Recently, chemical vapor deposition (CVD) using hydrocarbon plasma has been used to deposit carbon nanostructures²⁴ and oriented CNTs.^{25–27} In the above cases, except for Ref. 25, metal catalysts such as Ni and Fe were used to initiate and continue CNT and nanofiber growth.

In this paper, it is demonstrated that fibrous structures can be formed on diamond (CVD diamond films, single-crystal diamond, and diamond powder),²⁸ glasslike carbon,²⁹ and diamondlike carbon (DLC) films, when they are treated in hydrogen plasma that is generated by a 2.45-GHz microwave without magnetic field under a negative dc bias applied to the specimen at a moderate hydrogen gas pressure of 1.6 torr. This method will be referred to as negatively biased plasma (NBP) treatment hereafter in this paper. In the following, experimental details are described in Sec. II, results and discussion are presented in Sec. III, and conclusions are given in Sec. IV. It should be emphasized that in this work, no catalyst is necessary to form fibrous structures.

II. EXPERIMENTAL

A. NBP treatment

For a plasma generation using H₂, H₂ + O₂, or H₂ + CH₄, a microwave plasma generator system with a quartz-tube chamber was used, as shown in Fig. 1, which is widely used for CVD of diamond films.^{30–32} The specimen holder was made of Mo that can accommodate

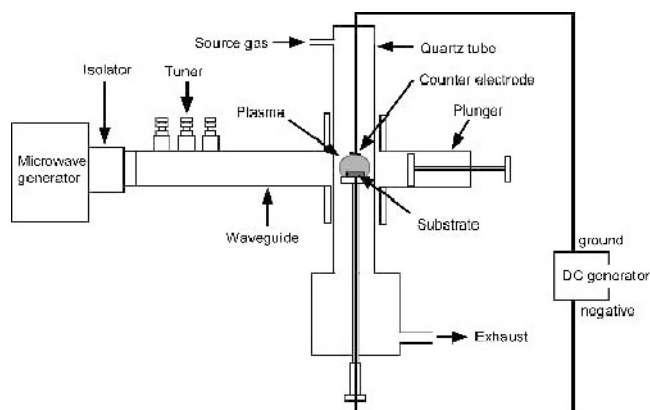


FIG. 1. Schematic structure of microwave plasma generator.

a 1×1 cm specimen, and the top surface was positioned more than 10 mm below the center of the wave guide. The holder was negatively biased with respect to a grounded W-ring counter electrode that was placed near the top edge of the plasma ball. Note that a similar setup is used for bias-enhanced nucleation (BEN) of diamond on Si.^{33–36} The present experiments were undertaken using two different plasma generation systems of the same type as shown in Fig. 1. Standard processing conditions were {approximately 1.6 torr, -200 to -300 V, 200–400 W, 500–700 °C} for the series I experiments using the first system and {approximately 1.6 torr, -150 to -300 V, 200–400 W, 300–500 °C} for the series II experiments using the second system. This pressure was the lowest attainable by the reactor used and was held at this value in most experiments, as the plasma was stable and the plasma ball was the largest. According to our preliminary examinations, however, it seemed that fibrous structures can be formed in a wider range of processing conditions, {e.g., ≤ 20 torr, ≤ -100 V, 200–600 W, RT}, although the precise limits have not been identified yet.

The specimen temperature T_s was measured through a quartz window located at the top of the chamber by an optical pyrometer. In the series I experiments, an optical pyrometer of single color with $\lambda = 0.9 \mu\text{m}$ was used in most cases, which can measure $T_s \geq 600$ °C. On the other hand, in the series II experiments, a new optical pyrometer (single color with $\lambda = 1.55 \mu\text{m}$) was used, which can measure T_s between 300 and 750 °C. Some experiments done in the series I experiments were then repeated using the new optical pyrometer, and it was concluded that $T_s \geq 500$ °C. Thus, when T_s was below 600 °C in the series I experiments, it will be often denoted as <600 °C, but it was actually $500 \text{ °C} \leq T_s < 600 \text{ °C}$. In all cases, no correction was made for the emissivity; i.e., the emissivity was assumed to be unity. This assumption is conventionally used for diamond CVD experiments, and thus T_s values described in this paper are

approximate. Finally, it must be noted that the above processing conditions for the NBP treatments are out of range for the CVD of usual polycrystalline diamond films, {i.e., 30–50 torr, 0 V, 300–600 W, 700–900 °C}, by the reactor of Fig. 1 using 0.2–5 vol% CH₄/H₂ as the source gas. Hence, there is no possibility that a few micrometer-size crystalline diamonds are formed by the NBP treatments.

The specimen temperature T_s became stable in about 10 min after the plasma ignition. The formation of fibrous structures however seemed to be quite insensitive to T_s , and occurred even when T_s was above 700 °C or down to 300 °C. The bias current was 10–50 mA and depended on the specimen position, P_m , V_b , and the W-ring shape and its position. In the present setup, the bias current is considered to occur by (i) a flow of positive hydrogen ions from the plasma to both the specimen and the specimen holder and (ii) electron emission from the specimen. Since part of the bias current due to hydrogen ions is considered to flow directly from the plasma to the Mo holder, the measured bias current does not at all represent the current passing only through the specimen. Even so, the bias current was found to be a good indicator to monitor the processing rate: the formation of the fibrous structure was faster when the bias current was higher. The biasing technique, BEN, has been widely used in CVD diamond research to synthesize highly oriented diamond (HOD) films, for instance.^{37–40} As is well known,⁴¹ under a negative bias at the specimen holder, a secondary plasma is generated over the specimen due to electron emission from the deposited diamond film. This was also the case in the present experiments. In case that the dc bias voltage was suddenly shut off, the specimen temperature dropped by about 40 °C, presumably because of the disappearance of both hydrogen ion collisions to the specimen and the secondary plasma.

The standard processing gas used was pure H₂ with a flow rate of 6–10 standard cubic cm/min (sccm), but gas mixtures of (i) H₂ + O₂ and (ii) H₂ + CH₄ were also used to study effects on fiber formation and morphology. The back pressure of the chamber was only about 10⁻⁴ torr, as rubber O-rings are used for vacuum seals. Under the processing conditions stated above, the plasma ball touches the quartz wall, and there was a possibility that silicon was included in the specimens. Impurity analyses however showed no indication of silicon inclusion in the fibrous specimens within the sensitivity limits. The major impurity was Mo from the specimen holder, and this issue will be described in more detail in Sec. III. The inner wall of the quartz tube was gradually covered with Mo as the experiments were repeated, which suppressed the transmission of the microwave and, hence, the formation of fibrous structures at the specimen surface. Thus, the quartz tube was replaced when a sign of non-reproducibility was noticed.

The distribution of fiber density and morphology over the 1 × 1 cm specimens was not always uniform, and very often, fibers were not formed in the central area of the specimen. To improve the uniformity of fiber density as well as fiber morphology, it was found that frequent rotation of the specimen during the NBP treatment was very effective. Particularly, it was most effective to do so every 1/2 to 1 min at the very beginning of the NBP treatment for 10 to 20 min. Even so, relatively minor changes in the fiber density and morphology existed across the specimen. Thus, scanning electron microscopy (SEM) images and other data in this paper were obtained from the central area of the specimens.

B. Specimens

Regarding materials for fiber formation, diamond films, single-crystal diamonds, diamond powder, glass-like carbon, and DLC films were used. Except for the single-crystal diamonds and the DLC films, the specimen size was 1 × 1 cm. The sample preparations are described in the following subsections.

1. Polycrystalline diamond films

Polycrystalline diamond films were deposited for 1 to 3 h to thicknesses of approximately 4 to 12 μm on low-resistivity *p*-type Si(100) substrates of 1 cm² by a 5-kW microwave plasma CVD reactor (ASTeX-type) using 2 vol% CH₄/H₂ as the source gas.⁴² The gas pressure and the specimen temperature were 120 torr and 850 °C, respectively. The film surface after 3 h mainly consisted of (111) and (100) faces of diamond grains with their edge lengths of 3 to 5 μm, as seen in Fig. 2. The film color was gray due to light scattering at the rough film surface. After an NBP treatment using H₂, the film surface appeared very dark, implying that the surface structure was significantly modified by the treatment.

HOD films were synthesized by a known procedure using BEN.^{37–40} The film surface consisted of (100) faces of diamond that were laterally aligned in almost the same direction, and hence, the film surface was quite flat. For HOD films used in the present experiments, however, randomly oriented, secondary nucleation of diamond existed at the film surface with an approximate density of 5 × 10⁶/cm². The film thickness was roughly 15 μm, estimated from the growth time.

2. Single-crystal diamond and diamond powder

The single-crystal diamonds (Sumitomo Electric Ind., Osaka, Japan) used were synthetic type Ib and 3 mm × 3 mm × 0.3 mm^t in size. It was transparent, but the color was yellowish due to nitrogen impurities. No fibrous structure was formed on this specimen by the NBP treatment, presumably because the diamond was electrically

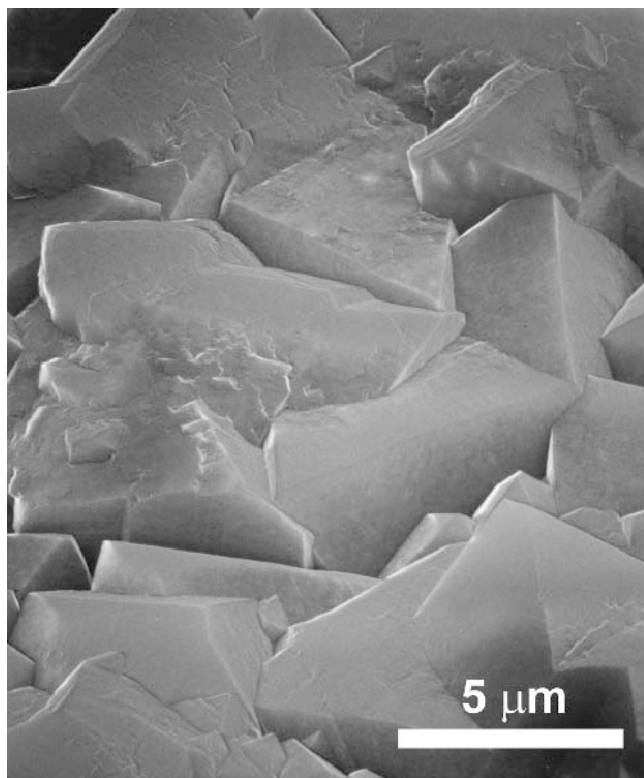


FIG. 2. SEM image of polycrystalline diamond film surface.

insulating. To solve this problem, a B-doped diamond layer was deposited on the single-crystal diamond for 24 h by the reactor shown in Fig. 1 using a mixture of 0.5 vol% CH_4/H_2 and 2 ppm B_2H_6 as the source gas. The layer thickness was estimated to be roughly 6 μm . As a result, fibrous structures were formed on the specimen surface by the NBP treatment. By contrast, no deposition of B-doped diamond layer was necessary to form fibrous structures by the NBP treatment on the surfaces of diamond powder (DeBeers, Ltd., Kobe, Japan 15–30 μm). They were manually spread over a low-resistivity *p*-type Si(100) substrate of 1 cm^2 and shaken off to leave isolated diamond particles sticking to the Si surface.

3. Glasslike carbon and DLC films

The glasslike carbon (Kobe Steel, Ltd., Kobe, Japan) was treated by hydrostatic isotropic press, sliced, and then mirror-polished. The specimens used were cut out of a large wafer to 1 cm \times 1 cm \times 0.80 mm^t. The untreated specimen appeared like a mirror but became very dark after an NBP treatment. DLC films of 3- μm thickness were deposited on Ti substrates (13 mm \times 13 mm \times 4.5 mm^t) by unbalanced magnetron sputtering⁴³ using an anisotropic graphite target 6 in. diameter in an Ar atmosphere of 3 mtorr. The dc power density was 0.057 W/mm², and the substrate bias was –200 V. Thus,

the DLC films used in the present experiments do not contain hydrogen unlike amorphous hydrogenated carbon (a-C:H) films.

C. Materials characterization

Among NBP-treated specimens of more than 200, some were characterized by SEM, infrared (IR), and Raman spectroscopy (the light source was a 514.5-nm Ar-ion laser), x-ray photoelectron spectroscopy (XPS), cathodoluminescence, Auger electron spectroscopy (AES), electron probe microanalysis (EPMA), electron energy loss spectroscopy (EELS), electron diffraction (ED), transmission electron microscopy (TEM), and high-resolution TEM (HRTEM). For XPS and AES, the measurement areas were 1.1 mm ϕ and 45 \times 60 μm^2 , respectively.

Measurements of ED and TEM were done at National Institute of Advanced Science and Technology (Tsakuba, Japan). The transmission electron microscope is equipped with an Ω -type energy filter, which allows a selection of electrons subjected to energy loss by transmission. The acceleration voltage was 200 kV. There was a difficulty in making TEM samples from diamond films with fibrous surfaces. Many different methods, including focused ion beam (FIB), were tested but were unsuccessful. This is because diamond films were very hard, and fibrous structures were very thin and unable to be detached from the basal diamond films. As a last resort, diamond specimens were vertically cut to a 100- μm width by a dicing saw, and the sample surface was observed by TEM from the side with a small tilt angle. Since deionized water was sprayed on the specimen during the dicing, the fibrous structures might be distorted. For glasslike carbon, the backside of the specimen was mechanically ground, dimpled, and then thinned by Ar-ion milling with an acceleration energy of 5 kV. The incident angle of Ar ions was set at 4° to prevent an ion damage. HRTEM measurements were carried out at Kobelco Scientific, Inc., (Kobe, Japan) using an acceleration voltage of 200 kV. In this case, the sample preparation was done by dicing both diamond and glasslike carbon specimens to a 100- μm width, and the fibers were observed from the side of the sample with a small tilt angle.

D. Field emission

Current–voltage (*I*–*V*) characteristics of field emission (FE) from specimens were measured at Kyoto University (Kyoto, Japan), while FE, field emission electron microscopy (FEEM), and photoelectron emission microscopy (PEEM) were done at North Carolina State University. In the former FE measurement system,⁴⁴ an Al plate was pushed on the edge area of the specimen surface for an electrical contact and the anode was a gold ball with a diameter of 2 mm. The specimen–anode distance was

variable by a piezoelectric rod, and the maximum applied voltage between the specimen and the anode was 250 V. In the latter case,^{45–47} a schematic diagram of the FEEM/PEEM system is shown in Fig. 3. The base pressure was less than 3×10^{-10} torr, the field of view is variable from 5 to 150 μm ϕ , the resolution was better than 15 nm, and the maximum applied voltage between the specimen and the anode was 20 kV across a gap of ≤ 4 mm. The flat part of the anode is about 1 cm ϕ , and the aperture diameter was 1 mm. The ultraviolet light source used was a Hg lamp, though a free electron laser source also was available. Measurements of I - V characteristics were also possible between the anode and the specimen, in which case all electrons emitted from the specimen of 0.36 cm^2 can be collected by the anode.

III. RESULTS AND DISCUSSION

The processing conditions, the objectives for specific experiments, and their major results are summarized in Table I, along with the specimen numbers. Note that in what follows, the thickness will be generally expressed by the superscript t .

A. Diamond

1. Polycrystalline diamond films

Figures 4(a)–4(d) show SEM images of a polycrystalline diamond film specimen of approximately 12- μm^t (see also Fig. 2) that have been NBP treated (No. 1 of Table I). Figure 4(a) shows a top view of the specimen. It is seen that fibers on the diamond film surface are

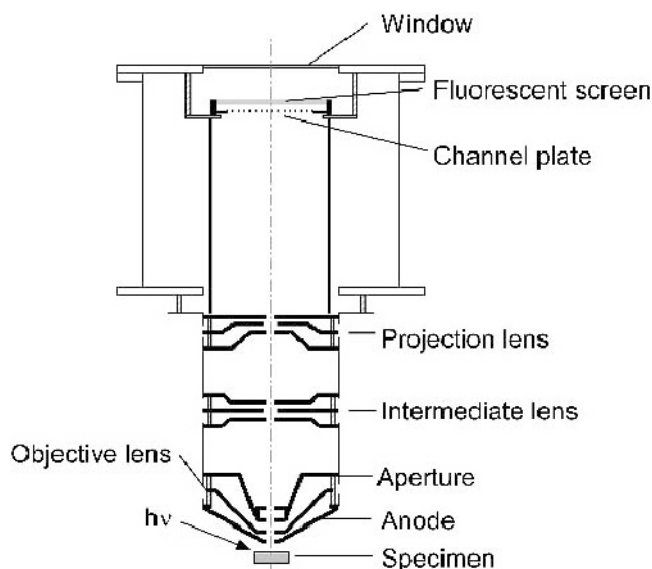


FIG. 3. Schematic diagram of the FEEM/PEEM system. The sample-anode distance is variable, and 2 or 4 mm was used in this work. The aperture diameter at the anode is 1 mm.

standing almost perpendicularly to the substrate plane, except for grain boundary areas in spite of the fact that the original faces of diamond grains were inclined with respect to the substrate plane. Figure 4(b) shows a surface view from 45° from the substrate normal. Such an angle will be simply referred to as “a viewing angle” hereafter. The elongation of the fibers, conformable to the initial granular diamond surfaces, is obvious. From a SEM image with a higher magnification (not shown), the fiber density was estimated to be 10^9 – $10^{10}/\text{cm}^2$. Figure 4(c) shows a SEM image of a fractured edge, where it is seen that 5- to 6- μm long fibers are formed. Hence, the average rate of fiber elongation was approximately 2 $\mu\text{m}/\text{h}$. It is of interest that the diameters of the fiber stems are approximately 1 μm , while the fibers are thinner toward the top ends. In most specimens of the series I experiments, where T_s was 500–700 °C, the fiber ends were smoothly extended as seen in Fig. 4(d) and the diameters in the top portion were less than 50 nm. There was no indication by SEM, TEM, and HRTEM on the presence of metal particles at the fiber ends, as will be seen later. In Fig. 4(d), it appears that the fibers are not hollow (tubular) but solid. It also appears in Figs. 4(a)–4(d) that fiber structures have been formed not solely by etching the diamond film but also by a growth from the diamond surface, presumably using hydrocarbon species generated by diamond etching. It is of great interest that the basal diamond film was etched despite the existence of about 5- μm^t fibrous layers.

To characterize fiber structures, Raman spectra of both *as-grown* (Fig. 2) and the NBP-treated specimen No. 1 (Fig. 4) were observed, and the results are shown by spectra a and b of Fig. 5, respectively. In both cases, there is an intense band at about 1334 cm^{-1} that is assigned to diamond and a broad band around 1500 cm^{-1} that is assigned to non-diamond carbon such as graphite and a-C:H.^{48,49} The full widths at half maximum for spectra a and b of Fig. 5 were 14 and 13 cm^{-1} , respectively. It is remarkable that the level of baseline for spectrum b was approximately half of that for spectrum a, presumably due to laser light absorption by the fibrous surface. In general, spectrum b is considered to contain Raman signals from both the fibers and the basal diamond, but it was not certain in this measurement to what degree the laser light went into fibers and scattered to be observed as Raman signals. In Fig. 5, the incident laser beam was only 5° tilted from specimen’s substrate normal. It has been increased to 20°, but there was no noticeable change in the spectrum. A similar Raman study is carried out in the next subsection, and more discussion will be given there.

Usually, IR absorptions due to C–H_x stretch vibrations are observed between 2800 and 3100 cm^{-1} for diamond films.^{48–52} Curves a and b in Fig. 6 show the IR spectra of an NBP-treated specimen and an *as-grown* polycrystalline film, respectively. In the former, only two

TABLE I. Summary of process conditions, objectives, and major results.

Specimen	Exp. series	Specimen ^a	Processing gas	<i>P</i> (Torr)	<i>V_b</i> (V)	<i>P_m</i> (W)	<i>T_s</i> (°C)	Treatment time	Objective	Corresponding figs.
No. 1	I	PCD (12 μm ²)	H ₂	1.6	-200	360	<600	3 h	Fiber formation	Fig. 4
No. 2	I	PCD (3 μm ²)	H ₂	1.6	-300	340	<600	20 min	Scratch test	Fig. 7
No. 3	I	HOD (10 μm ²)	H ₂	1.6	-300	370	<600	1 h	Fibers on HOD	Similar to Fig. 9
No. 4	II	PCD (4 μm ²)	H ₂	1.6	-300	370	<600	11 h	Long time treatment	Fig. 8
No. 5	I	B-doped layer on SCD Ib (100)	H ₂	1.5	-300	400	<600	40 min	Fibers on SCD	Fig. 9
No. 6	II	Diamond powder	H ₂	1.6	-150	380	415	3 h	Fibers on powder	Fig. 10
No. 7	I	PCD (4 μm ²)	H ₂	1.6–1.8	-300	370	<600	5–40 min	Fiber formation process	Fig. 11
No. 8	I	PCD (12 μm ²)	H ₂	30	-300	385	670	2 h 40 min	Higher <i>P</i>	Fig. 12
No. 9	I	PCD (12 μm ²)	10% CH ₄ /H ₂	1.9	-200	400	<600	3 h	CH ₄ addition	Fig. 13
No. 10	I	PCD (12 μm ²)	20% CH ₄ /H ₂	1.9	-300	370	520	27 min	Higher CH ₄ concn.	Fig. 14
No. 11	I	PCD (12 μm ²)	10% CH ₄ /H ₂	10	-200	400	<600	1 h	CH ₄ addition at higher <i>P</i>	Fig. 15
No. 12	II	PCD	H ₂	1.6	-200 to -300	~400	300–400	~1 h	Low <i>T_s</i>	Thin and frizzy fiber ends
No. 13	I	PCD	H ₂	1.8	-300	470	630	1 h	High <i>T_s</i>	Thick fibers with round tops
No. 14	I	PCD (12 μm ²)	H ₂	1.4	-400	300	<600	1 h	High <i>V_b</i>	Low fiber density
No. 15	I	PCD (12 μm ²)	0.5 sccm O ₂ + 10 sccm H ₂	2	-200	450	<600	4 h	O ₂ addition	No fiber, rough surface
No. 16	I	B-doped PCD (3 μm ²)	H ₂	1.6	-200	360	610	1 h	B-doped film	Complete etching due to fast reactions
No. 17	II	PCD	H ₂	1.6	+200	380	420	2 h	Positive bias	Short fibers
No. 18	CVD	Specimen No. 1	0.3% CH ₄ /H ₂	50	0	400	800	1 h	Diamond CVD on fibers	Diamond coating on fibers, Fig. 16
No. 19	II	Specimen No. 10	H ₂	1.6	-150	390	420	50 min	Fiber formation on nanocrystalline diamond film	Small and dense fibers in addition to the dropletlike structures of Fig. 14
No. 20	I	PCD	H ₂	1.6	-300	470	<600	1 h	EELS, ED	Figs. 17 and 18
No. 21	I	PCD	H ₂	1.6	-300	380	<600	3 h	HRTEM	Fig. 20
No. 22	I	GLC	H ₂	1.7	-300	370	<600	30 min	Conical structures	Fig. 21
No. 23	I	GLC	H ₂	1.6	-200	360	<600	1 and 3 h	Raman	Fig. 22
No. 24	I	GLC	H ₂	1.6	-200	380	<600	3 h	TEM, ED	Figs. 23–25
No. 25	I	GLC	H ₂	1.6	-300	370	<600	1 h 20 min	HRTEM	Fig. 26
No. 26	II	DLC	H ₂	1.6	-200	380	420	36 min	Conical structures	Similar to Fig. 21(a)
No. 27	I	GLC	H ₂	1.6	0	380	<600	1 h 30 min	No bias	No structure
No. 28	I	GLC	H ₂	1.8	-200	370	<600	3 h	Conical structures	
	CVD	GLC with fibers	1% CH ₄ /H ₂	50	0	370	800	3 h	Diamond CVD	Fig. 27
No. 29	II	GLC	1.4% O ₂ /H ₂	1.6	-200	390	410	1 h	Fibrous structures	Fig. 28

^aPCD: polycrystalline diamond film. HOD: highly oriented diamond film. SCD: single-crystal bulk diamond. GLC: glasslike carbon. DLC: diamond-like carbon film.

peaks exist at 2856 and 2913 cm⁻¹. On the other hand, three absorption peaks are seen at 2819, 2850, and 2925 cm⁻¹ in the latter. Note that, in these spectra, constant backgrounds were subtracted from the original spectra to highlight the absorption band shapes. It was found that the absorption intensity of spectrum a is approximately three times greater than that of spectrum b, indicating that fibrous specimen contains C–H_x bonds at the surfaces and within the fibers. According to Refs. 48–52, the 2856- and 2913-cm⁻¹ bands in spectrum a can be assigned to *sp*³ CH₂ symmetric and asymmetric stretching vibrational modes, respectively. Similarly, the 2850- and 2925-cm⁻¹ bands in spectrum b can be assigned to the same modes, respectively. The 2819-cm⁻¹ band was not uniquely assigned but can be a vibrational mode of either O–C–H,⁵⁰ O–CH₃, N–CH₃,⁵¹ or diamond (111)-H.⁵² The IR spectrum a of Fig. 6 for the NBP treated specimen indicates that *sp*³ CH₂ structures are most abundant in the fibers.

To qualitatively examine the adhesion strength of the fibers to the basal diamond, the surface of the NBP treated specimen No. 2 was scratched by a tweezers edge. Figure 7 shows a SEM image of the scratched area, where the scratch line passes from the bottom right to the top left on the fibrous surface with fiber lengths of roughly 3 μm. It is obviously seen that fibers were not detached from the basal diamond film but only bent, implying that the fibers are atomically continuous from the basal diamond film. The two bright areas in Fig. 7 are where fiber groups were uniformly bent, and the secondary electron emission was intense, probably because incident and secondary electrons can reach the fibers without deflection by the dense fibers. Indeed, the side view of the fibers by SEM also appeared bright in Fig. 4(c).

A NBP treated HOD film No. 3 also had a fibrous surface similar to that shown in Fig. 4. The fiber lengths as well as the fiber morphology were however more uniform so that the fiber ends were well aligned, as the

initial surface of HOD film was fairly flat. A magnified SEM view that was similar to Fig. 9 will be shown in Sec. III. A. 2.

To see how the fibrous structures change after a long time treatment, a NBP treatment No. 4 was done for 11 h. A SEM image of the specimen surface is shown in Fig. 8. It is seen that the surface consisted of fibrous structures, but most of them are strongly bent in the middle, and fairly thick and wide stems support the thin frizzy fibers. A SEM view of a fractured edge (not shown) appeared very similar to Fig. 4(c) except that the fibers had more complex shapes due to bending. It was

also seen that the diamond film was etched down to the Si substrate, and the stems and thin fibers form an approximately $4\text{-}\mu\text{m}^2$ layer. This result indicates that during the NBP treatment using H_2 , the basal diamond film was subject to etching, even though such a thick fibrous layer was present at the specimen surface, as seen in Fig. 8. This makes one imagine a surprising process that hydrogen ions pass through the dense layer of fibers, reach the surface of basal diamond film, and react with diamond to make chemically active hydrocarbon species, which move up along the fibers, and some reach fiber ends to make them longer. Meanwhile, the fibrous structures

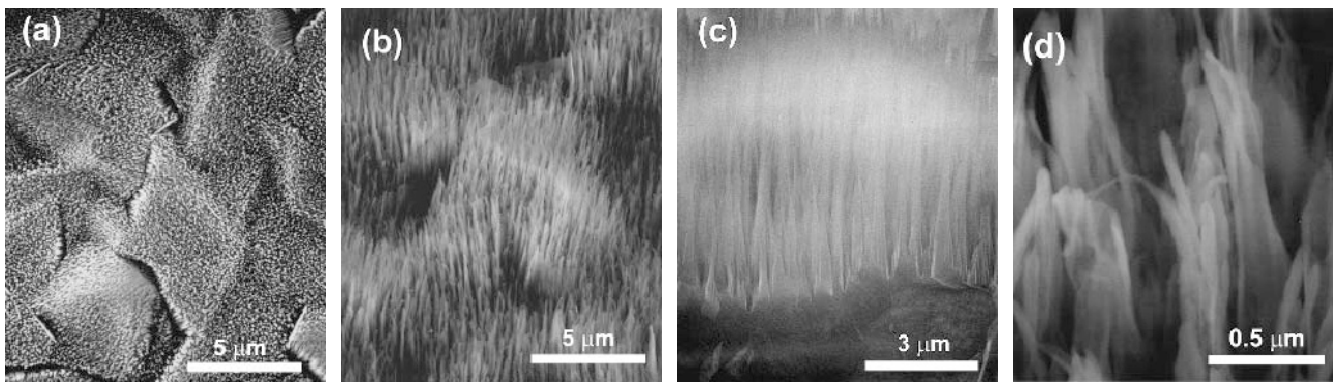


FIG. 4. SEM images of polycrystalline diamond film surface (No. 1): (a) top view, (b) viewing angle of 45° , (c) fractured edge, and (d) a magnified view of the fiber ends with a viewing angle of 45° .

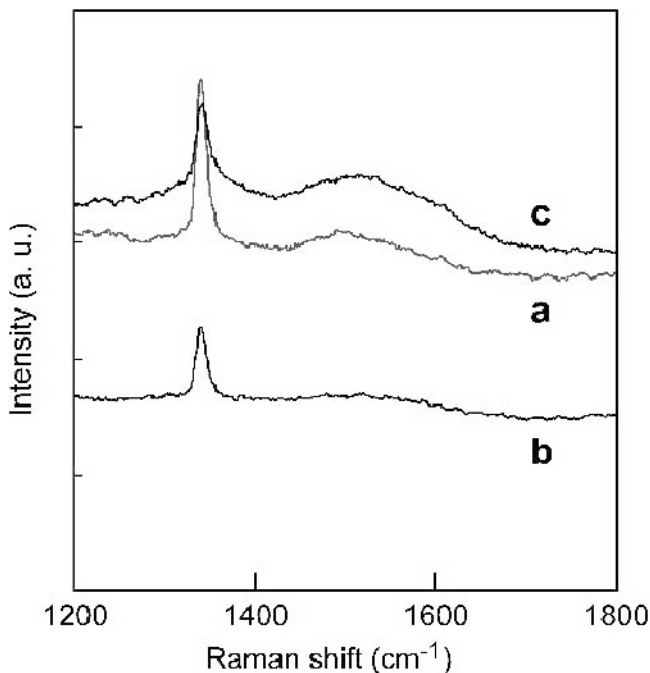


FIG. 5. Raman spectra of (a) untreated polycrystalline diamond film (Fig. 2), (b) NBP treated diamond film with a fibrous surface (Fig. 4), and (c) NBP-treated diamond film after diamond CVD (Fig. 16). No background subtraction was made.

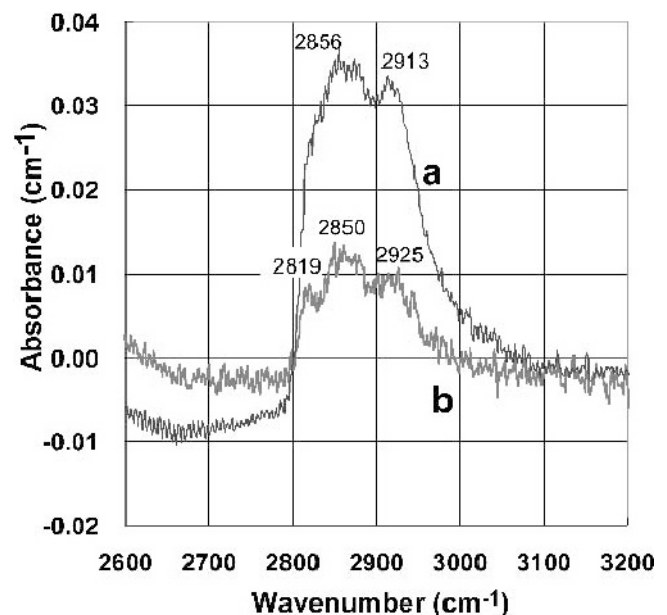


FIG. 6. Infrared spectra of (a) NBP treated diamond film with a fibrous surface and (b) as-grown diamond film, both on Si substrates.



FIG. 7. SEM image of the scratched area at a fibrous surface of diamond film (No. 2). The viewing angle is 45°.

themselves were basically intact despite the fact that they were constantly exposed to the hydrogen plasma under dc bias.

2. Single-crystal diamond and diamond powder

The inset of Fig. 9 shows a SEM image of the NBP-treated single-crystal diamond Ib, No. 5. As stated in Sec. II. B. 2, fibers were not formed on an insulating diamond crystal by the NBP treatment but on a B-doped diamond layer deposited on the diamond crystal. The fact that to form fibers the specimen must be conducting, either via bulk or surface, indicates that the bias voltage plays an important role for fiber formation. It is of interest to compare the inset of Fig. 9 with Fig. 4(b): the heights of the fiber ends are more uniform in the former case because the initial diamond surface was flat. The color of the NBP-treated specimen was lightly dark but semi-transparent. The solid and dotted curves in Fig. 9 correspond to the Raman spectra from the diamond surfaces with and without fibrous structures, respectively. It is observed that there is no significant difference in the spectra between the two sides except that the peak intensity at 1333 cm^{-1} on the reverse side without fiber was 11% higher. This can be understood in the same way as in Fig. 5 that the Raman scattering from the fibrous side

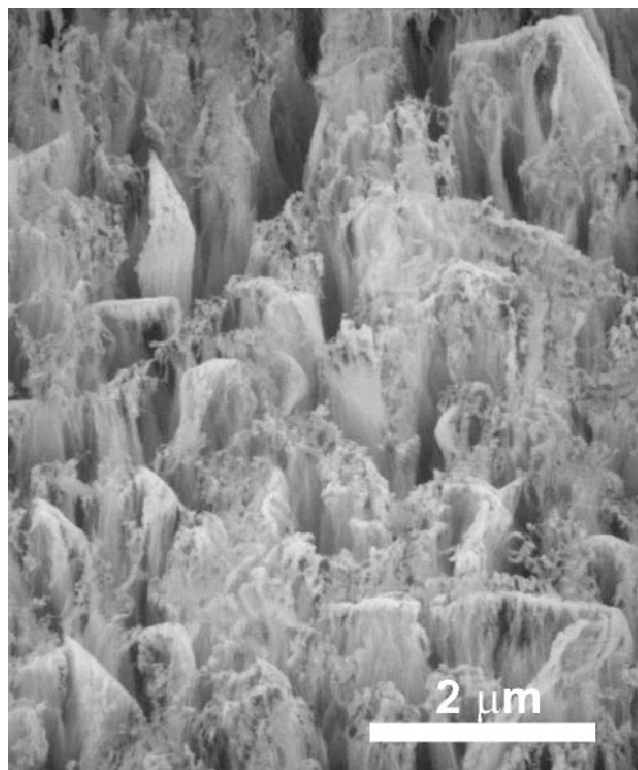


FIG. 8. SEM image of diamond film that has been NBP treated for 11 h (No. 4). The viewing angle is 30°.

is weaker. Note that, in the Raman spectra of both surfaces, there was no band due to non-diamond components in the $1400\text{--}1600\text{ cm}^{-1}$ region. From these and the previous results of Sec. III. A. 1, it follows that (i) the fibers do not contain non-diamond components detectable by Raman spectroscopy and, hence, (ii) the band around 1500 cm^{-1} in Fig. 5(b) for a NBP treated polycrystalline diamond film arises from the basal diamond film and not from the fibers, if the assumption is the case that Raman signals from the fibers are detected in both Figs. 5 and 9.

A NBP treatment No. 6 was undertaken for diamond powder, and a SEM image of particle surfaces is shown in Fig. 10. Similar to the result of Fig. 4, the particle surface was converted to a fibrous structure, where the fibers are aligned along the direction normal to the substrate surface. It is remarkable that virtually all fibers, even those at the side surfaces of the diamond particle, are unidirectionally aligned, implying that the electric field due to the dc bias determines the fiber direction. It should however be mentioned that the fiber morphology of a different powder specimen that had been NBP treated under conditions of {1.7 torr, -200 V , 500 W , $<600\text{ °C}$ } for 6 h using hydrogen plasma in the series I experiments was considerably different from the results of Fig. 10: the fiber diameter was approximately $0.25\text{ }\mu\text{m}$, and their ends were round.²⁸

3. Fiber formation process

To investigate the process of fiber formation, four different undoped diamond films were NBP treated, No. 7, for 5, 10, 30, and 40 min, and the specimen surfaces were observed by SEM. The results are shown in Figs. 11(a)–11(d). All SEM images were taken from a viewing angle of 20°. As seen in Fig. 11(a), protuberant structures with approximate diameters of less than 0.1 μm and heights of 0.2 μm were created only after a 5-min exposure of the diamond film to the hydrogen plasma. After 10 min

[Fig. 11(b)], the heights of protuberances increased to 0.4 μm and small fibrous structures were visible. It appears that fibrous materials were created along the side surface of each protuberance toward the center. After 30 min [Fig. 11(c)], the protuberances had diameters of about 0.5 μm and were further elongated to be the fibrous structures of about 1 μm in height. There is a certain distribution in the height of the protuberances, and not all have fibrous structures. After 40 min [Fig. 11(d)], the surface had a typical fibrous morphology, similar to Fig. 4(b), and the fiber lengths were now

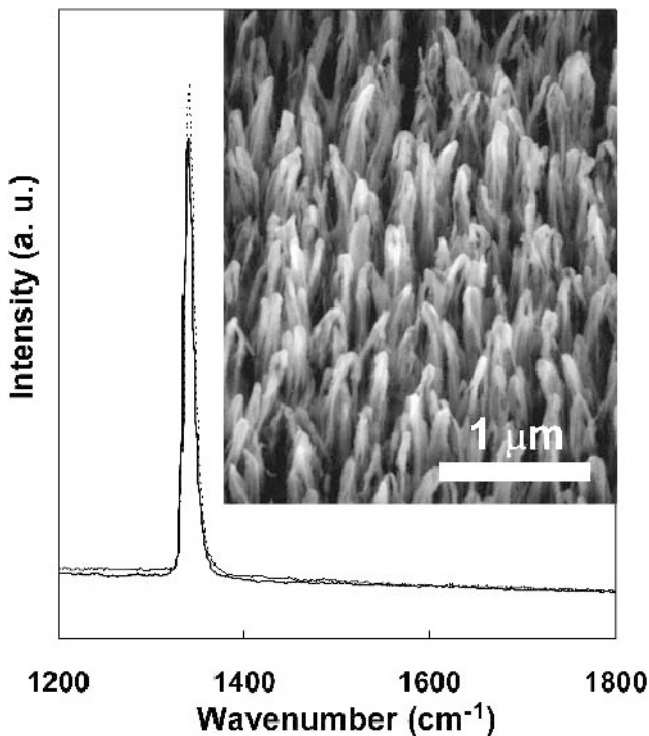


FIG. 9. Raman spectra of single-crystal diamond. The solid curve is the spectrum of the NBP treated surface (No. 5) that has been deposited with a B-doped diamond layer by CVD. The dotted curve is the spectrum of the reverse side of the crystal without fiber. The inset is a SEM image of the NBP-treated surface. The viewing angle is 45°.

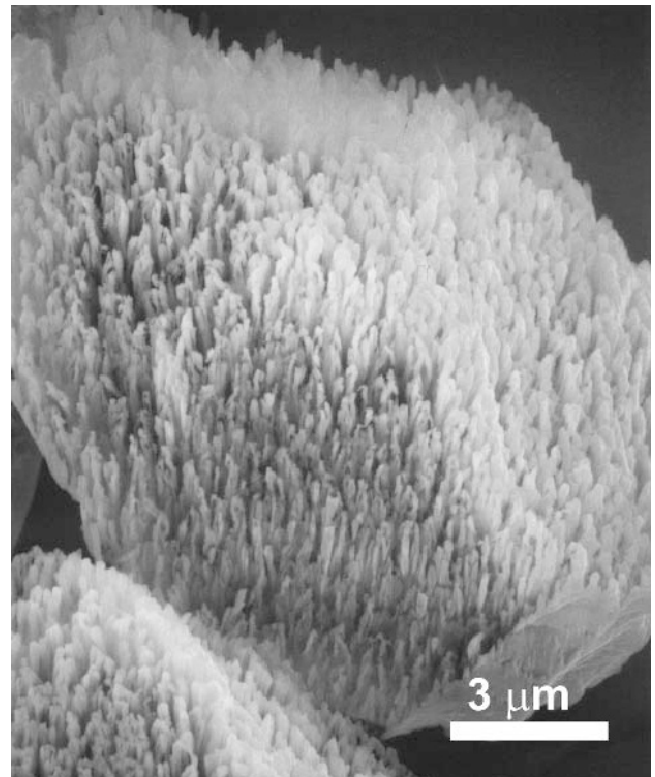


FIG. 10. SEM image of diamond particles that have been NBP treated (No. 6). The viewing angle is 30°.

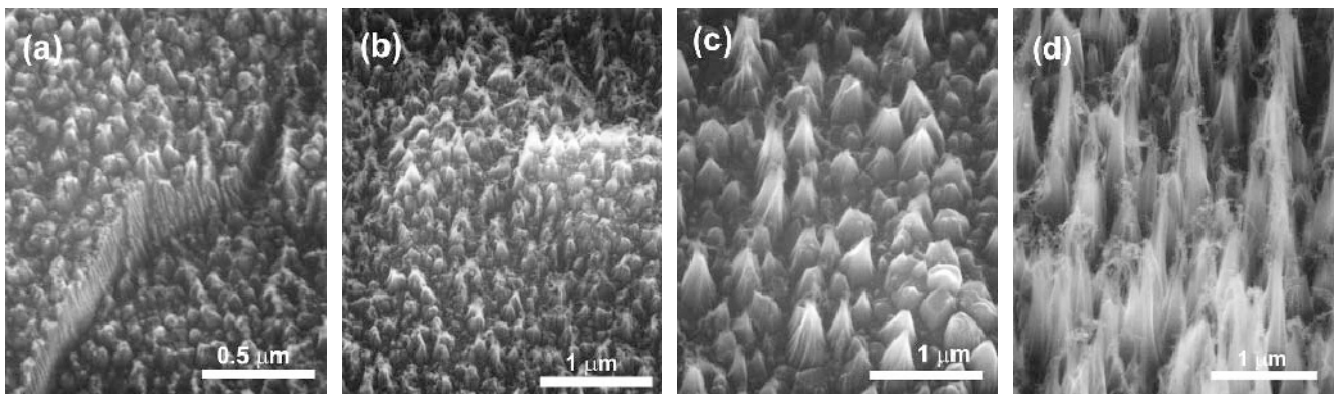


FIG. 11. SEM images of NBP treated diamond films (No. 7) after (a) 5 min, (b) 10 min, (c) 30 min, and (d) 40 min. The viewing angles are 20°.

about 2 μm . There exist however frizzy structures at the top of the fibers. Above results show that the uneven etching of diamond surface in the initial stage to form protuberances, followed by a fiber formation and their elongation, is the basic process to finally end up with the fibrous morphology of Fig. 4. In Figs. 11(a)–11(d), it is of great interest that the diamond film is etched and eroded, but the fibrous structures are not only intact but also grown under the biased hydrogen plasma environment.

4. Effects of gas pressure

To study the effects of gas pressure on fiber formation, and also confirm the results of Jiang *et al.*,^{8,9} an undoped diamond film was NBP treated, No. 8. Like in experiments at $P \sim 1.6$ torr, a secondary plasma was observed over the specimen by biasing. A SEM image of the specimen surface is shown in Fig. 12. It is seen that the film surface was severely etched by hydrogen plasma, leaving bunched steplike structures on grain surfaces. This result is consistent with those of Refs. 8 and 9. As seen in Fig. 12, there is no fibrous structure at the film surface. It is thus concluded that the fibrous structure is formed only when diamond is NBP treated at a pressure at least below 30 torr.

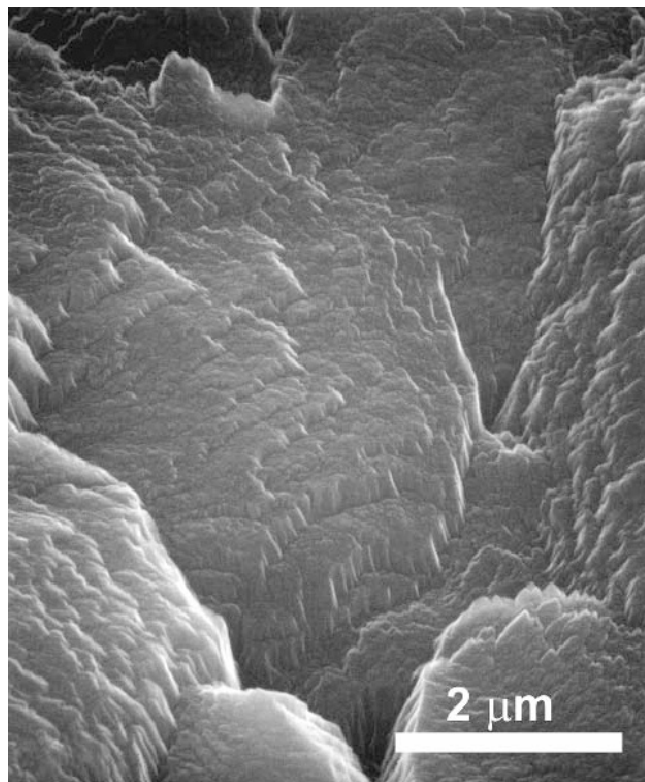


FIG. 12. SEM image of a diamond film surface after the NBP treatment No. 8 at 30 torr. The viewing angle is 30°.

5. Addition of CH_4 to the processing gas

So far, it was pure hydrogen that was used for NBP treatments of diamond. It is thus considered that the carbon source for fiber formation is chemically active hydrocarbons produced by etching diamond with hydrogen plasma. In this section, CH_4 gas, as an external carbon source, was added to hydrogen, and changes in the fibrous structures were examined. In the first experiment No. 9, 10 vol% CH_4/H_2 was used for the NBP treatment. Figure 13 shows the resulted structure at the film surface observed by SEM. It is seen that fibrous structures were formed on the film surface instead of carbon or DLC film deposition. From a comparison of Fig. 13 with both Figs. 4(d) and the inset of Fig. 9 using magnified SEM images (not shown), it was found that the outer shape of each fiber appeared fuzzier. The fiber density of Fig. 13 was approximately $10^{10}/\text{cm}^2$, slightly higher than the cases of Figs. 4 and 9 without CH_4 addition. It is hence inferred that the density of protuberances [Fig. 11(a)] also was higher. It is of interest that, in the center of Fig. 13, there is a flat face where there is no fiber. This is due to the fact that this face is standing almost perpendicularly to the substrate surface, and thus, the bias effect was not operational on this surface. Similar phenomena have been observed for different specimens with and without CH_4

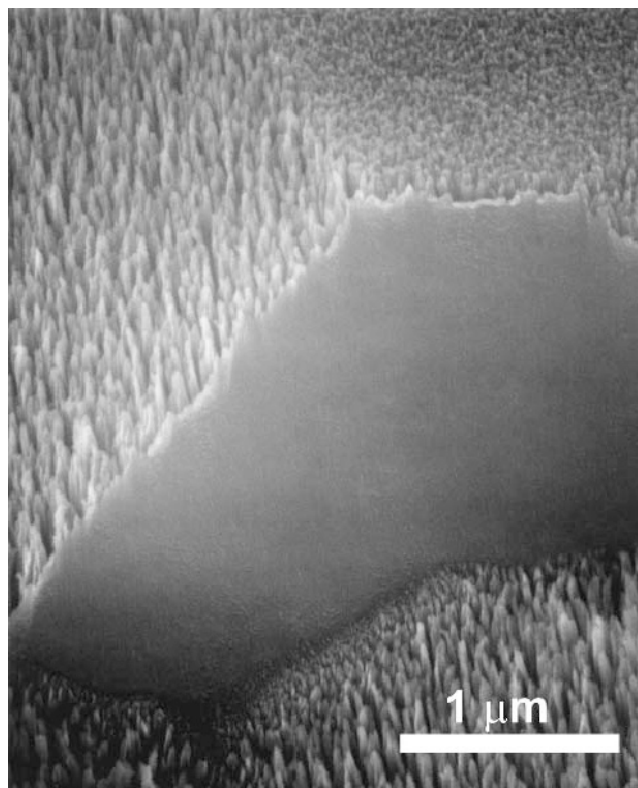


FIG. 13. SEM image of diamond film surface after the NBP treatment No. 9 using 10 vol% CH_4/H_2 as a processing gas. The viewing angle is 45°.

in the processing gas. This result implies that reactive collisions of positive hydrogen ions to the diamond surface along the electric field, which is nearly perpendicular to the substrate surface, trigger the fiber formation.

In the second experiment No. 10, 20 vol% CH₄/H₂ was used for the NBP. The SEM image of the specimen surface is shown in Fig. 14. It appears that the initial diamond surface was covered by both a-C:H or DLC layer and granular particles. Small fibrous structures were about to grow from some granules. In this case, it seems that carbon was oversupplied from CH₄ in the processing gas, and fiber formation due to diamond etching did not occur.

In the third experiment No. 11, a NBP treatment was done using 10 vol% CH₄/H₂ at 10 torr. The resulted surface, observed by SEM, is shown in Fig. 15. It was found that fibrous structures were also formed in this case. Unlike the results of Figs. 4 and 9, however, the fiber ends are not straight but twisted in a complex manner. This can be understood in such a way that carbon nanoparticles generated from CH₄ decomposition are deposited on the sidewalls of the fibers to make the directions of fiber elongation more random. If this assumption is actually the case, it follows that the fiber growth by the NBP treatment without CH₄ addition takes place via such

transport processes as electromigration or thermal diffusion of carbon species, which have been generated by hydrogen plasma etching of basal diamond film, along the sidewall of the fibers.

6. Various effects of experimental factors on fiber formation

In this section, effects of some experimental factors on fiber formation are described. Since comprehensive studies on the issues have not yet been done, only qualitative descriptions will be given below: No. 12, when T_s was low (300–400 °C), the fiber ends became thinner and frizzy. No. 13, by contrast, when T_s was high in such a case that the specimen was placed in the center of the wave guide, the fibers were thick and their ends were rounded. No. 14, when a high bias voltage of –400 V was applied for a polycrystalline diamond film, most of the film were etched out, leaving vertically standing fibers along a network of distorted circles. It was presumed that the locations of the circles correspond to grain boundaries of the polycrystalline diamond films used. No. 15, upon addition of 0.5 sccm O₂ to 10 sccm H₂, no fiber was formed by the NBP treatment, and the film surface was etched and roughened. Namely, the presence of a small amount of oxygen in the processing gas prevents the fiber formation. No. 16, it was found that B-doped

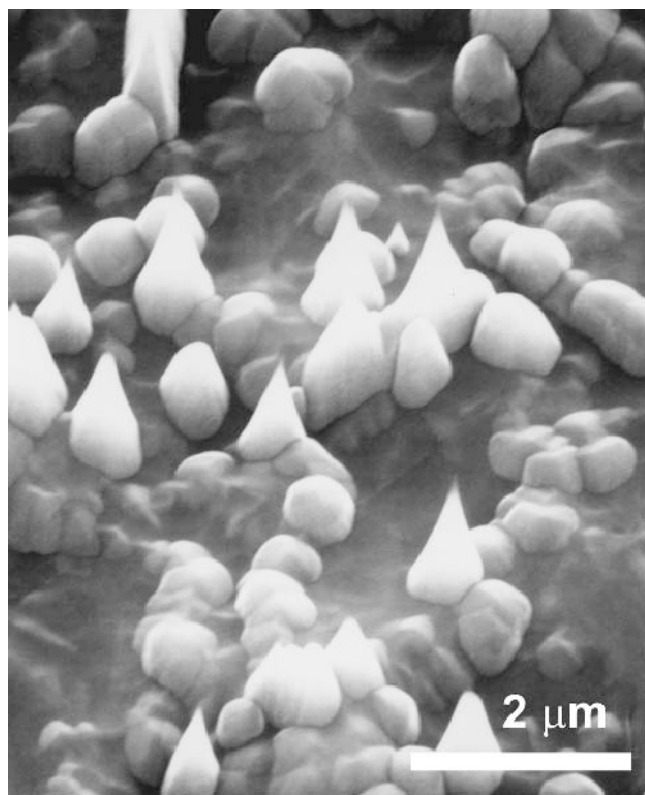


FIG. 14. SEM image of diamond film surface after the NBP treatment No. 10 using 20 vol% CH₄/H₂ as a processing gas. The viewing angle is 30°.

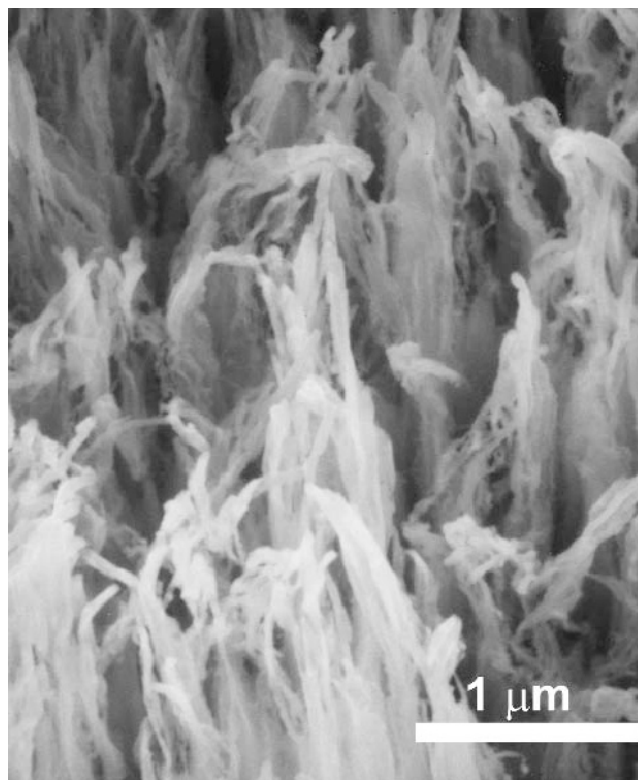


FIG. 15. SEM image of diamond film surface after the NBP treatment No. 11 at 10 torr using 10 vol% CH₄/H₂ as a processing gas. The viewing angle is 45°.

diamond films were etched much faster than undoped ones, though fibrous structures were formed on B-doped diamond films before they were completely etched. For instance, a 3- μm^{\dagger} B-doped diamond was completely etched out after 1 h.

The experimental results presented in Secs. II. B. 2 and III. A. 2 indicate that to form fibrous structures on the diamond surface by the NBP treatment, the diamond specimen must be conducting. B-doped diamond films obviously fulfill the condition. For the case of as-grown undoped polycrystalline diamond films made by CVD, it is known that there exists a surface conducting layer due to hydrogen termination.^{53–62} Unlike these cases, fibrous structures were not formed on bulk Ib diamond because it is insulating. It is however known that hydrogen-plasma-treated bulk diamond surface is conducting;^{53–62} i.e., the bulk Ib diamond should be conducting in hydrogen plasma during the NBP treatment, but this contradicts the experimental result of Sec. III. A. 2. By contrast, fibrous structures were formed on diamond powder without pretreatment. Although detailed investigation has not been done yet, it is considered that the electrical contact of the bulk diamond with the Mo holder was poor under the present experimental setup because the reverse surface of the bulk diamond is insulating, while it was opposite for diamond powder, as the path length from the Si substrate to the top surface of the particle is shorter and presumably a reaction took place between diamond powder and Si to form SiC at the interface, which helped reduce the interface resistance.

A similar experiment was undertaken by applying a positive bias to the polycrystalline diamond film under conditions of No. 17 in Table I. It was found that the diamond surface was roughened and seemed to consist of short fibers with a length of roughly 50 nm. This can be attributed to the fact that hydrogen, activated by electrons incident from plasma, caused the etching of diamond film.

7. Diamond CVD on fibers

In this section, a fibrous specimen of Fig. 4 was processed by diamond CVD using the reactor shown in Fig. 1 under conditions of No. 18 listed in Table I. The purpose of this experiment was to know the nature of the fibers. Namely, if the fiber has a diamond structure, it will be uniformly coated with diamond by CVD. On the other hand, if the fiber is graphitic or a-C:H, the fiber will be etched or no diamond is deposited on it under the conditions of No. 18.

The experimental results were as follows: The color of the specimen was dark before the diamond CVD due to the fibrous structures at the surface but became gray after the CVD. The SEM photographs of the specimens after CVD are shown in Figs. 16(a) and 16(b). In Fig. 16(a), the specimen was strongly charged up at this

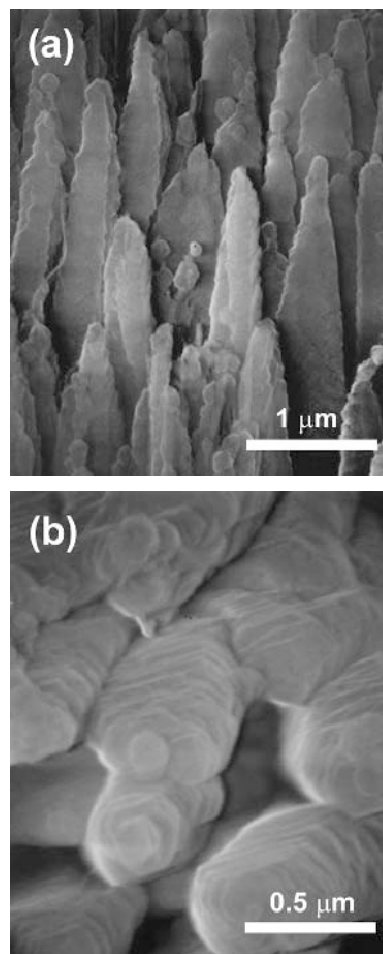


FIG. 16. SEM images of fibrous surface after diamond CVD, No. 18: (a) viewing angle of 30°; (b) a top view.

magnification, but it is seen that each fiber was uniformly coated with diamond. The fiber diameter near the end is now 0.3–0.5 μm . In Fig. 16(b), diamond facets are clearly visible. These micrographs show that there was no preferential growth of diamond on fiber ends. It is however seen in Fig. 16(a) that there are diamond particles of 0.1–0.2 μm in diameter at some of the fiber ends: namely, the fiber ends can be nucleation centers of diamond. The fiber density estimated from SEM images was $5 \times 10^8/\text{cm}^2$, significantly smaller than the initial fiber density of 10^9 – $10^{10}/\text{cm}^2$. This is presumably because multiple fibers were coalesced together by diamond CVD. The Raman spectrum of the specimen is shown in spectrum c of Fig. 5. It is noticed that the background level of spectrum c now is almost the same as that of spectrum a for an untreated diamond film, indicating that the specimen surface with thickened fibers scatter laser Raman light as efficiently as the untreated diamond film does. Apart from the background level, the broad 1500- cm^{-1} band of spectrum c is more

intense than spectra a and b, and the main peak at 1335 cm^{-1} has a broader foot. This is presumably because the grain sizes of the new diamond layer, coating the fibers, are smaller than those of the untreated diamond film (Fig. 2), and hence, the diamond layer includes more nondiamond components in the grain boundaries.^{63–65}

It is of interest to see if the fibrous structure can be formed on the surface of nanocrystalline diamond film or a-C:H film, i.e., on nanocrystalline carbon materials. To study this, an NBP treatment was carried out using the specimen shown in Fig. 14 under conditions of No. 19, as the basal surface of the specimen of Fig. 14 was nanocrystalline or amorphous. It was found that the resulting surface consisted of dropletlike structures, similar to those seen in Fig. 14, sitting on a layer of small and dense fibers. This indicates that fibrous structures can also be formed on nanocrystalline diamond films or a-C:H films.

8. Surface impurity analyses

To check the presence of impurities at the fibrous specimen surface, AES, XPS, and EPMA measurements were undertaken. The AES results showed the presence of C (77.3 at.%), O (17.9 at.%), and Mo (4.8 at.%). It was considered that the O signal was originated from O_2 adsorbed in air and Mo was from the specimen holder. Similarly, XPS showed the presence of C (79.8 at.%), O (16.8 at.%), and Mo (3.4 at.%). The Mo signal consisted of three bands that were assigned to molybdenum oxides. Since the NBP treatment was done in hydrogen plasma, it seemed that the oxidation of Mo occurred after the specimen was taken out of the chamber and exposed to air. In both AES and XPS measurements, Si was not detected (below the detection limits). It might then be questioned if the formation of fibrous structures was initiated by the presence of Mo micromasks. This does not however seem to be the case for the following two reasons: (i) Fig. 11(a) indicates a formation of protuberant structures that does not seem to be originated by the micromasking. (ii) In Sec. III. A. 9, the fibrous structures were observed by TEM and HRTEM and showed no indication on the presence of Mo particles. To avoid the presence of Mo impurity, one can use, for instance, a graphite holder rather than Mo. In this case, however, the graphite itself is etched by the hydrogen plasma in the NBP treatment, as will be seen in Sec. III. B, and thus hydrocarbon species will be generated in the plasma in an uncontrollable manner. The hydrocarbon concentration depends on the NBP treatment conditions, which can influence the fiber morphology, and causes problems in the reproducibility of the experiment. In contrast to XPS and AES data, EPMA measurements resulted in the atomic concentration ratio of C (95.2 at.%), O (4.4 at.%), Si (0.2 at.%), and Mo (0.1 at.%), the Mo impurity

concentrations being extremely smaller than those of XPS and AES. This is presumably because EPMA included the signal from the basal diamond region as well as the fibrous structures at the surface.

As is well known, the Auger band shape for carbon depends on the allotropes (diamond, graphite, and amorphous carbon). In the present measurement, the band shape was more similar to amorphous carbon rather than diamond. This suggests that the fiber surface is covered by an amorphous carbon layer. Indeed, it will be seen that this is actually the case.

9. EELS, ED, TEM, and CL analyses

The fibrous structures of diamond specimens were studied by EELS, ED, TEM, and HRTEM. For sample preparation, see Sec. II. C. An EELS spectrum of carbon K-edge of the fibrous structure is shown in Fig. 17, where the spectra on the right-hand side show typical EELS

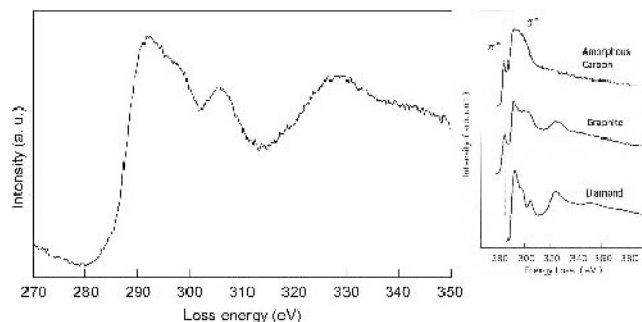


FIG. 17. EELS spectrum of a NBP treated diamond film with a fibrous surface. The spectra on the right-hand side show corresponding spectra for various carbon materials.

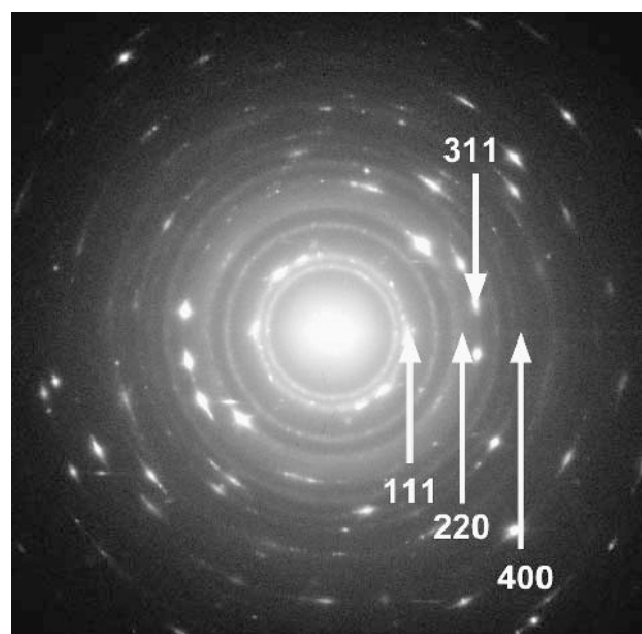


FIG. 18. Electron diffraction from the fibrous structure of diamond film.

spectra for various carbon materials. The NBP treatment conditions used to make the specimen are No. 20 in Table I. In Fig. 17, the π^* peak at 284 eV is absent, which indicates that sp^2 and sp bonds are not included in the fibrous structure. The bands observed between 300 and 340 eV are the near-edge structure of carbon atoms, common to all carbon materials. Thus, the EELS spectrum showed that the fibrous specimen is diamond. Figure 18 shows a selected-area ED pattern from the same specimen. The observed spotty ring patterns, indicated by arrows, can be assigned to diamond. This means that the diffraction area of the fibers contained a few diamond crystallites. The observed lattice constants were 2.08, 1.28, 1.07, and 0.89 Å, which are in good agreement with the lattice constants of diamond, 2.060 Å for (111), 1.261 Å for (220), 1.075 Å for (311), and 0.892 Å for (400). Other continuous diffraction rings were attributed to molybdenum oxides.

The fibrous structures were also observed by low- and high-resolution TEM. As already stated in Sec. II. C, there was difficulty in sample preparation, because the fibers could not be scratched off from the basal diamond film. Thus, the specimen was vertically cut to a width of about 100 μm by a dicing saw, and the fiber portion was observed from a small tilt angle. Other methods such as FIB were unsuccessful so far. Figure 19 shows a low resolution TEM zero-loss image of the same specimen as above. The zero-loss image, which was filtered with a window width of $\delta E = 15$ eV at a loss energy of $\Delta E = 0$ eV, was obtained from both unscattered and elastically scattered electrons so that the Bragg scattering and phase

contrast were enhanced better than the unfiltered image. It is seen in Fig. 19 that the typical diameter of the fibers was 50 nm, consistent with the SEM image of Fig. 4(d). It is also seen that the fibers are nanocrystalline, as indicated by ED of Fig. 18, and a number of defects, such as twins and stacking faults, are present in each crystallite. Furthermore, it appears that the fiber surfaces are covered with amorphous layers.

Figure 20 shows part of a HRTEM image of a fiber that has been treated under conditions of No. 21. The acceleration voltage of the electron beam was 200 kV. This figure shows more clearly that the fiber consisted of a crystalline core (labeled by C) covered with amorphous layers (labeled by A), as described above. Despite the statement in Sec. II. C that the very end of the fiber might be distorted during the sample preparation, it was concluded from the entire HRTEM image (not shown) that the basic feature of the fiber structure was retained, meaning that the damages by sample preparation were minimal. The lattice spacings in the crystalline regions, evaluated from the HRTEM image, were 1.9 and 2.5 Å, which are in fair agreement with the (111) spacing (2.060 Å) and the (110) spacing (2.522 Å) of diamond, respectively. The results of ED and HRTEM that the fibers have diamond structure are consistent with the fact that the fibers are uniformly coated with diamond by CVD, as seen in Fig. 16.

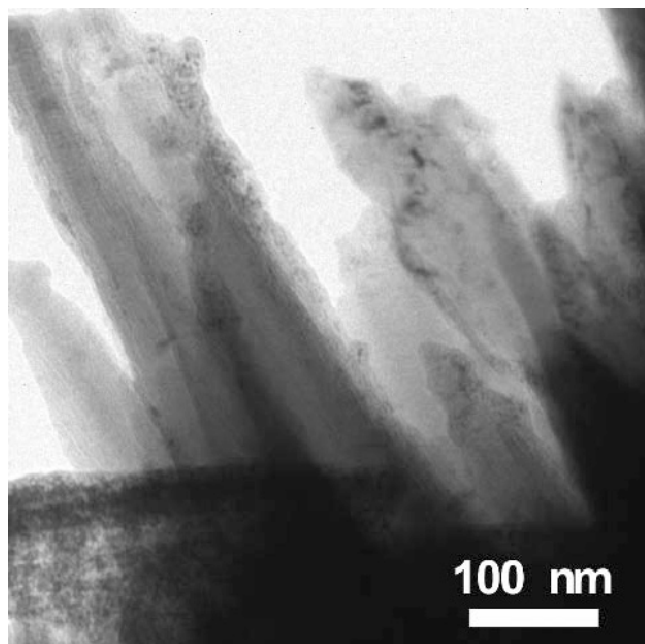


FIG. 19. Low-resolution TEM image of fibers formed on diamond film by NBP treatment.

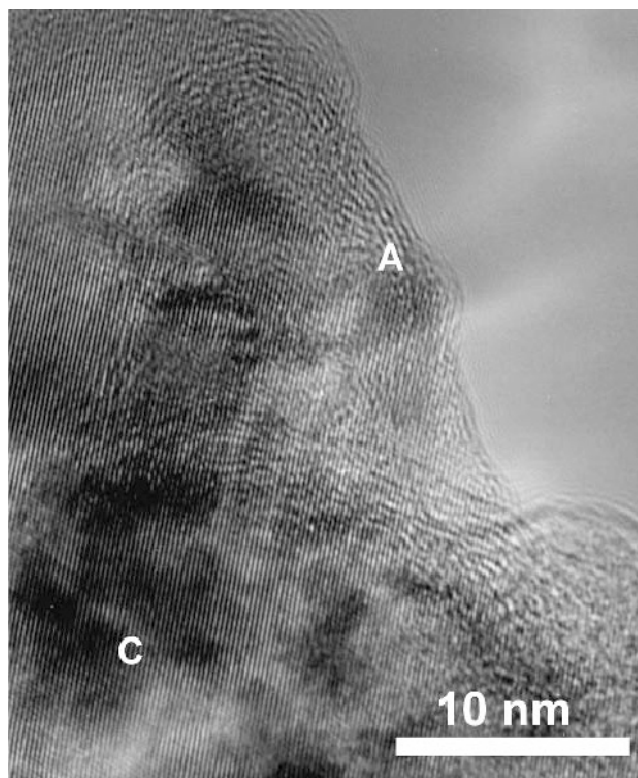


FIG. 20. Part of HRTEM image of a fiber formed on diamond film by NBP treatment.

Cathodoluminescence spectra of both polycrystalline diamond film and a fibrous specimen were observed between 200 and 800 nm at room temperature to see if there are any signals arising from fibrous structures. Unfortunately, both specimens exhibited similar spectra: there was only one symmetric band at 425 and 421 nm for the polycrystalline diamond film and the fibrous specimen, respectively. The peak intensity for the polycrystalline diamond film however was approximately 8 times higher than that for the fibrous specimen. This is presumably due to the fact that electron-hole pair generations are limited in the thin fibers, and there are more nonradiative processes in the fibrous specimen because of a higher density of defects.

B. Glasslike carbon and DLC films

1. Glasslike carbon

Experiments similar to those described so far for diamond were carried out for glasslike carbon described in Sec. II. B. 3. Figures 21(a) and 21(b) show SEM images

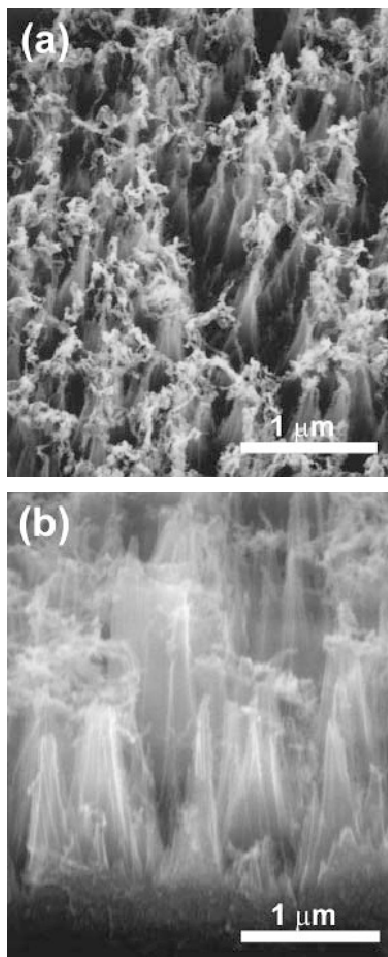


FIG. 21. SEM images of conical structures of glasslike carbon formed by the NBP treatment: (a) surface structure with the viewing angle of 30°; (b) fractured edge.

of the surface and a fractured edge of a NBP-treated specimen No. 22, respectively. It can be seen that the surface of the mirror-polished glasslike carbon was

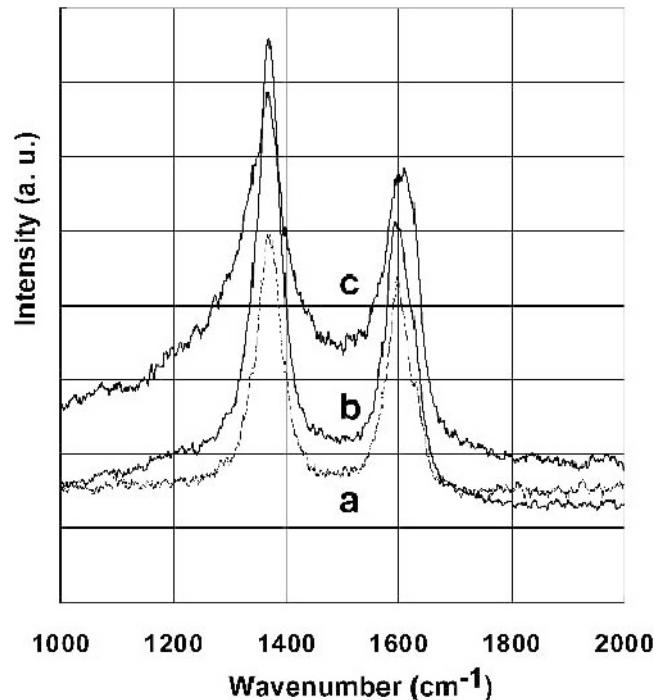


FIG. 22. Raman spectra of glasslike carbons: (a) untreated, (b) NBP treated for 1 h (No. 23), and (c) NBP treated for 3 h (No. 23).

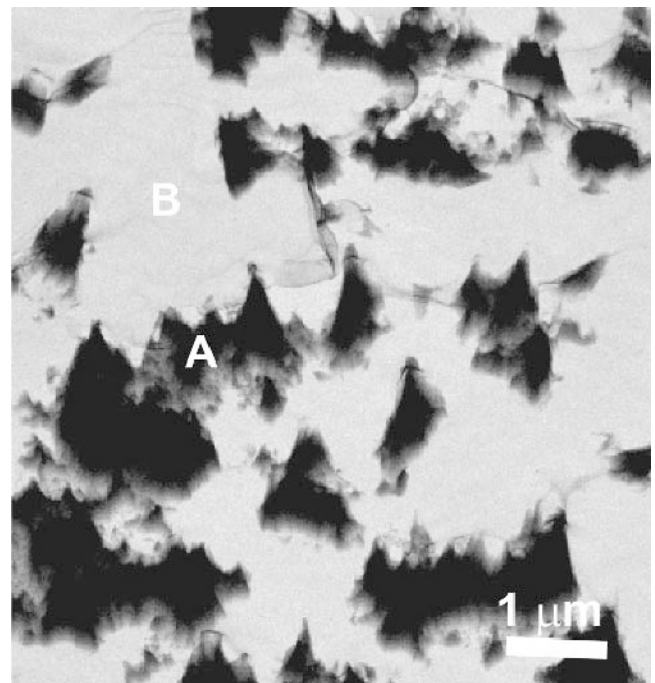


FIG. 23. Low-magnification TEM image of NBP treated glasslike carbon surface (No. 24). Area A contains conical structures, and area B is the basal surface. Both areas were observed by ED.

converted to an irregular conical morphology by the treatment, where the cone diameter near the top end was ≤ 50 nm and the cone heights were about $1 \mu\text{m}$ as seen

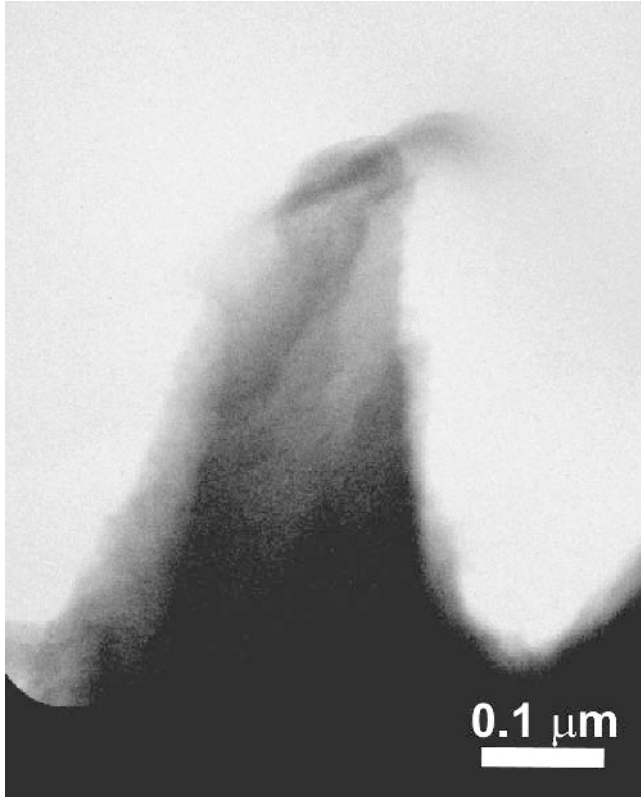


FIG. 24. Magnified TEM view of the top portion of the conical structure in area A of Fig. 23.

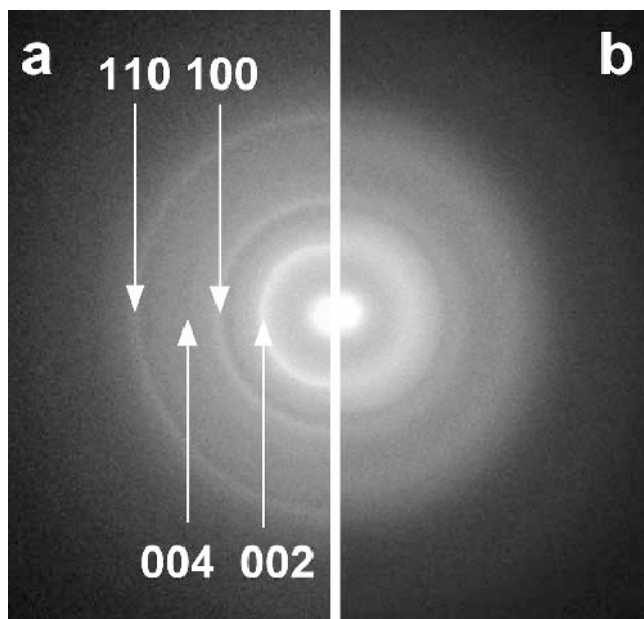


FIG. 25. ED patterns of (a) area A with fibrous structure and (b) basal surface area B.

in Fig. 21(b), although the cone ends were strongly frizzy. The density of conical structures was evaluated to be about $10^9/\text{cm}^2$ from a SEM image (not shown).

Raman spectra of an untreated glasslike carbon and NBP-treated (No. 23) glasslike carbons are shown in spectra a–c of Fig. 22, respectively. In reference to spectrum a for the untreated specimen, the basic features of the spectra b and c of the NBP-treated specimens were similar, consisting of two bands of graphite at 1380 and 1600 cm^{-1} . It should however be noted that, for spectrum a, the 1380-cm^{-1} band is sharp, while, for spectrum c, the 1380-cm^{-1} band has a tail toward the smaller wave number side. This result suggests that the conical structures consist of nanocrystalline graphitic particles.³⁰

Figure 23 shows a zero-loss image of a low-resolution TEM for a NBP treated (No. 24) glasslike carbon. Since carbon is soft, the backside of the specimen was dimpled down and thinned by an Ar-ion beam, as described in Sec. II. C. Figure 23 shows a view of the edge area observed from the front side with a tilt angle of 29.3° from the surface normal. The presence of conical structures is clearly seen. Figure 24 shows a magnified TEM image of a top portion in a cluster of conical structures seen in area A of Fig. 23. The conical structure has bottom and top diameters of 520 and 80 nm, respectively. The frizzy structure at the top end also is obviously seen.

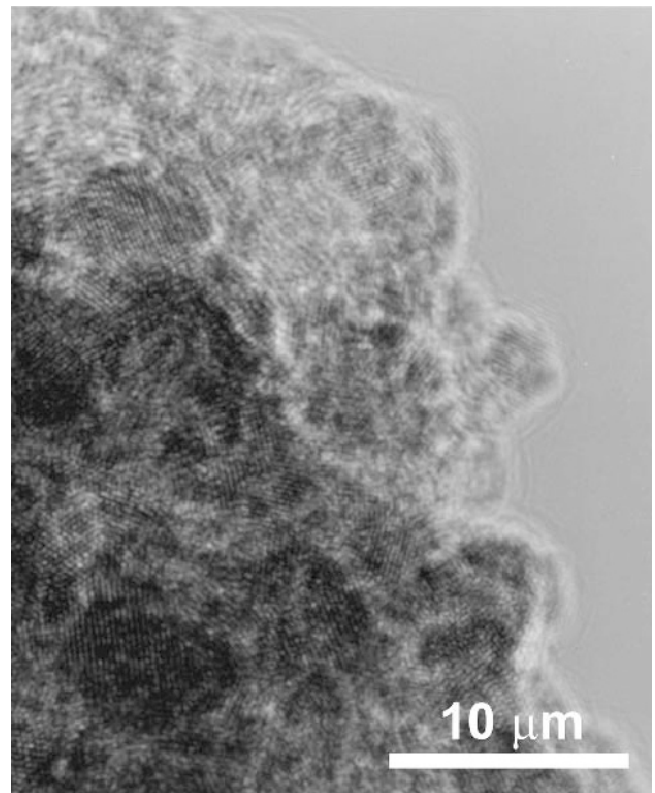


FIG. 26. HRTEM image of the fiber end.

The selected-area ED patterns, taken from approximately $1\text{-}\mu\text{m}$ ϕ areas indicated by A and B in Fig. 23, are shown in Figs. 25(a) and 25(b), respectively. The ED pattern from area A was obtained from the conical structures and shows a ring pattern of hexagonal close packed structure with observed lattice constants of 3.43, 2.12, 1.72, and 1.23 Å, which can be assigned to (002) of 3.38 Å, (100) of 2.12 Å, (004) of 1.68 Å, and (110) of 1.23 Å of graphite. The reflection indices of the rings are also given in Fig. 25(a). The ED result also shows that the conical structure is fine-grained graphite. On the other hand, the ED pattern from area B, shown in Fig. 25(b), was obtained from the basal glasslike carbon and shows a halo pattern. This means that the basal carbon became amorphous by the NBP treatment.⁶⁶

Figure 26 shows a HRTEM image of a fiber end. The NBP treatment conditions used are listed in No. 25 of Table I. It is seen that the fiber consisted of nanocrystals of graphite structure, consistent with the ED result. The diameters of the nanocrystals are less than 10 nm. In a different specimen, however, the fiber structure observed by HRTEM was amorphous, although the NBP treatment conditions were the same as above except that the treatment time was 1 h.²⁹ Thus, it seems that the atomic

arrangement in the conical structure sensitively depends on NBP treatment conditions as well as the details of the experimental procedure.

2. DLC films

A DLC film of 10 mm ϕ and $3\text{-}\mu\text{m}^t$ was deposited by unbalanced magnetron scattering, as described in Sec. II. B. 3, which was then NBP treated under conditions of No. 26. It was found that the film surface was converted to conical structures similar to Fig. 21(a). This demonstrates that conical structures can be formed at the surfaces of both bulk- and thin-film carbon. NBP treatments were also applied for carbon paste painted with different thicknesses on Si substrates without postannealing. As a result of NBP treatments, the surfaces were extremely roughened, but it was found by SEM that fuzzy conical structures also were formed.

3. Various effects on conical structure formation

To examine the effects of dc bias on the surface structure of glasslike carbon, a hydrogen plasma treatment was carried out without dc bias under conditions of No. 27. It was found that no fiber was formed, as expected. Next, like in the case of Sec. III. A. 7, a conical carbon specimen was made under conditions of No. 28 and successively a diamond CVD was undertaken using conditions of No. 28. It was found that only a featureless

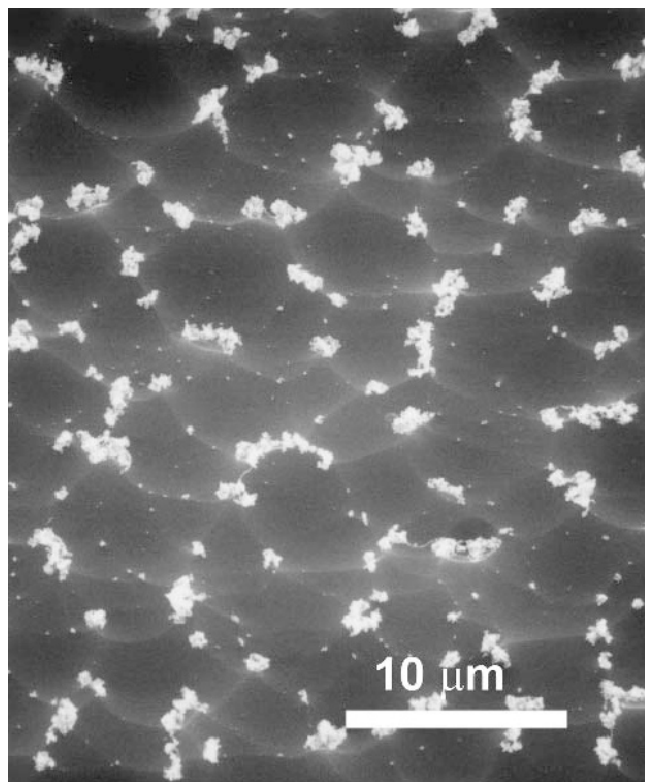


FIG. 27. SEM image of the surface after diamond CVD. The initial surface was similar to the one shown in Fig. 21. The viewing angle is 45° .

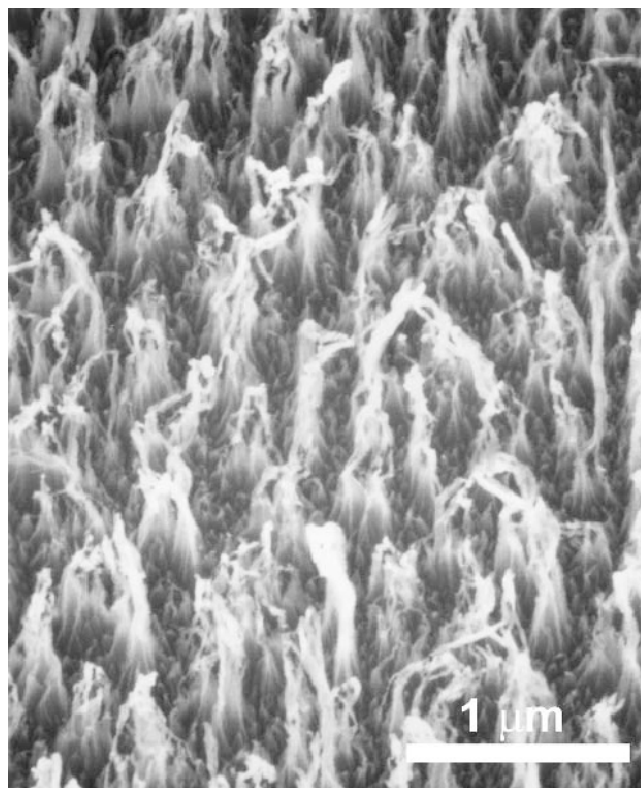


FIG. 28. SEM image of the surface that was NBP treated using 1.4 vol% O_2/H_2 for 1 h (No. 29). The viewing angle is 30° .

surface was formed as shown in Fig. 27. The conical structures created by the NBP treatment disappeared completely after the diamond CVD, and a wavy surface with small aggregates at the tops resulted. This is consistent with the fact that the fibers were graphitic, which is more easily etched by hydrogen plasma than diamond.³²

To investigate the effect of increased etching rate of carbon on surface morphology, a NBP treatment was undertaken by adding 1.4 vol% O₂ in H₂ under conditions of No. 29, and the SEM image of the resulted surface is shown in Fig. 28. It is seen that, unlike Fig. 21, the surface structure is fibrous rather than conical. Since the carbon etching rate by oxygen plasma is higher than hydrogen plasma, the formation of fibrous structures in Fig. 28 is attributed to the increased etching rate. Namely, it was found that the surface morphology can be controlled to some extent by adding O₂ in the standard processing gas, H₂.

C. Field emission

1. Field emission from NBP-treated diamond films

Since NBP-treated diamond films have fine fibrous structures at the surfaces, it would be of interest to examine how field emission of electrons is affected by the fibrous structures. First, standard *I*-*V* measurements

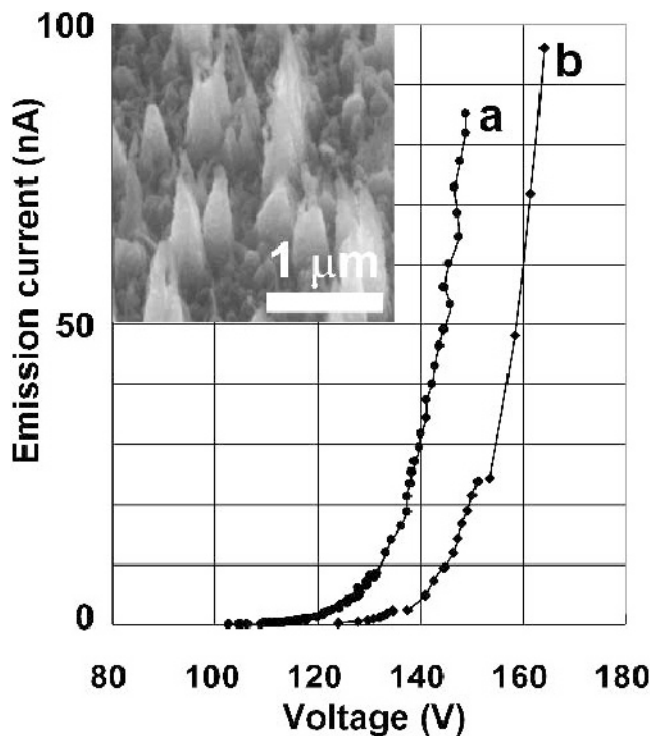


FIG. 29. Field emission *I*-*V* characteristics of (a) a fibrous diamond film specimen and (b) a B-doped polycrystalline diamond film. The inset is a SEM image of the specimen surface with a viewing angle of 45°.

were undertaken using a system stated in Sec. II. D,⁴⁴ where the anode was a gold ball with a diameter of 2 mm. The distance between the anode and the specimen is variable by a piezoelectric device, and the results described below were obtained when the distance was 1.5 μm. Prior to the measurements, an aging of the specimen was done by maintaining a low current emission overnight. The observed result is shown in Fig. 29. The specimens used were a NBP-treated fibrous diamond specimen (curve a) and a B-doped polycrystalline diamond film (curve b). In the former case, a SEM image of the fibrous specimen is shown in the inset of Fig. 29. To make this specimen, (i) a 3-μm^t undoped diamond film was first deposited using 0.5 vol% CH₄/H₂ as the source gas and the same type of reactor as shown in Fig. 1 for 12 h, (ii) a NBP treatment was done under conditions {1.6 torr, -300 V, 460 W, 520 °C}, (iii) a diamond CVD was undertaken using 0.5 vol% CH₄/H₂ and 1 ppm B₂H₆, and (iv) finally, a NBP treatment was again carried out for 1 h under conditions of {1.6 torr, -200 V, 380 W, 500 °C}. This somewhat complicated procedure was used to make the fibrous specimen electrically conducting. On the other hand, the latter specimen was synthesized by the same reactor using 0.5 vol% CH₄/H₂ and 1 ppm B₂H₆ at 60 torr for 12 h. The film thickness was estimated to be about 2 μm. The film surface consisted of diamond grains 0.5–1 μm in diameter. It is seen in Fig. 29 that the threshold voltage for field emission is approximately 20 V lower for the fibrous specimen than the polycrystalline diamond film, indicating that the presence of the fibrous structure increased the field emission efficiency. Their Fowler–Nordheim plots (not shown) were linear, consistent with the field emission from the surface.

Figures 30(a) and 30(b) show FEEM and PEEM images of a B-doped polycrystalline diamond film without and with a Hg lamp illumination, respectively. The viewing areas were 50-μm φ for both cases, and 20 kV was applied across a 4-mm gap between the specimen and the planar anode. The B-doped diamond film was synthesized using 0.5 vol% CH₄/H₂ and 0.25 ppm B₂H₆ as the

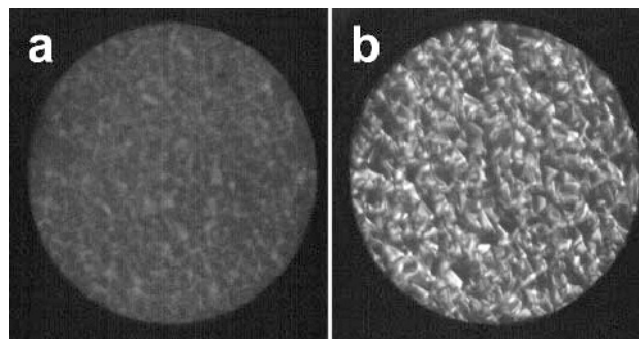


FIG. 30. (a) FEEM and (b) PEEM images of B-doped polycrystalline diamond film.

source gas under conditions of {50 torr, 0 V, -400 W, 800 °C} for 12 h. The film thickness was roughly 2 μm . It is seen that the field emission is markedly increased by the Hg lamp illumination as electrons are excited by the UV light. It is also seen that the electron emission is more intense at the tops and the edges than the flat faces of diamond grains.

Figures 31(a) and 31(b) show SEM and PEEM images, respectively, of a NBP-treated B-doped polycrystalline diamond film with a fibrous structure at the surface. The PEEM image of Fig. 31(b) also has a 50- μm ϕ viewing area on the specimen with an applied voltage of 20 kV under a Hg lamp illumination. The fibrous specimen was made in a similar manner as above: (i) First, a 3- μm^2 undoped polycrystalline diamond film was NBP treated under conditions of {1.6 torr, -300 V, 460 W,

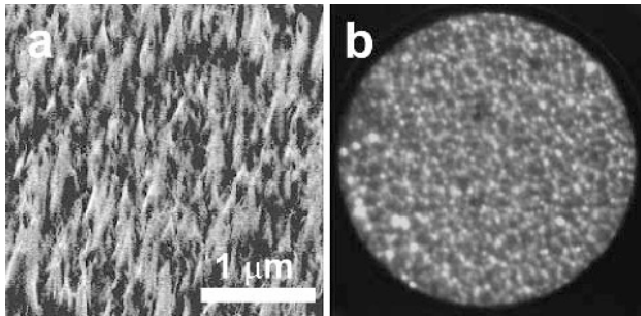


FIG. 31. (a) SEM and (b) PEEM images of B-doped diamond film with fibrous structures at the surface.

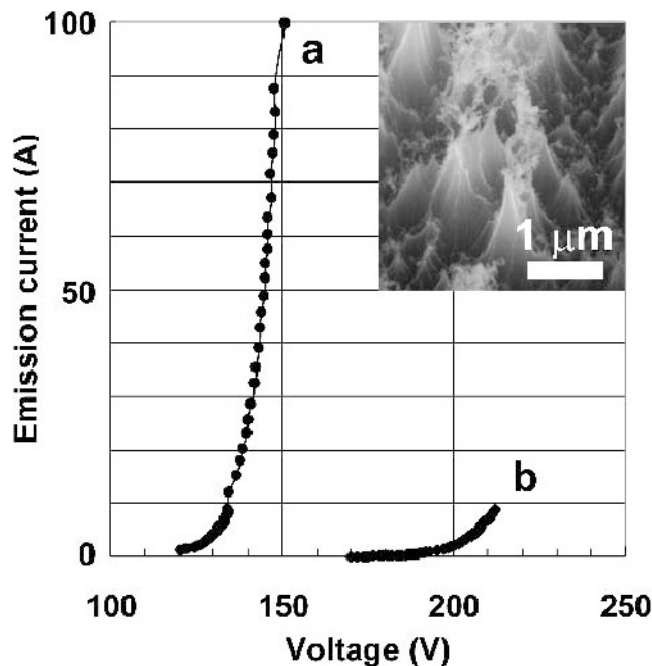


FIG. 32. Field emission I - V characteristics of (a) a conical carbon specimen and (b) untreated specimen. The inset is a SEM image of the fibrous specimen surface with a viewing angle of 45°.

590 °C} using hydrogen plasma for 30 min in the series I experiments. (ii) A B-doped diamond layer was deposited using 0.5 vol% CH_4/H_2 and 1 ppm B_2H_6 for 1 h. And then (iii) the specimen was again NBP treated by hydrogen plasma for 1 h under conditions of {1.6 torr, -300 V, 460 W, <600 °C} to form fibrous structures as seen in Fig. 31(a). It was found that the FEEM image (not shown) was dark, while in the PEEM image of Fig. 31(b), the electron emission occurs from each end of the fibers.

2. Field emission from NBP-treated glasslike carbon

In this subsection, I - V and FEEM measurements of the NBP-treated glasslike carbon were undertaken. The experimental setup and procedure for I - V measurements are the same as before, and the observed results are shown in Fig. 32, where the inset is a SEM image of the specimen used. In the figure, curve a is the result for the fibrous specimen and curve b is that for untreated glasslike carbon whose surface was mirror polished. It is obviously seen that the emission current is higher and the threshold voltage is lower for the NBP-treated specimen than the untreated one.

Figure 33 also shows I - V characteristics measured using the FEEM system for a NBP-treated conical specimen and an untreated glasslike carbon, respectively. As a pretreatment, the NBP-treated specimen was annealed in the vacuum of the FEEM system at 150 °C for 24 h under

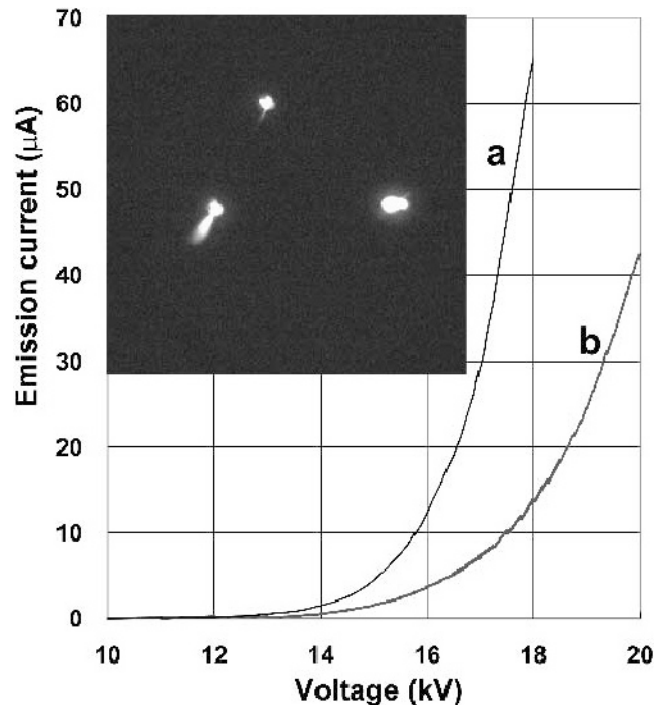


FIG. 33. Field emission I - V characteristics of (a) a carbon specimen with conical structures and (b) an untreated specimen observed by the FEEM system. The inset is a FEEM image of NBP-treated glasslike carbon surface.

an applied voltage of 20 kV with an anode–specimen distance of 4 mm. In the I – V results, the current was due to electron emission from a 0.36-cm^2 specimen, and all electrons were collected by the planar anode. Like the I – V results described on diamond, the emission current for the NBP-treated specimen was significantly higher because of the fibrous structures. A result of FEEM is shown in the inset of Fig. 33, where the observed area is $150 \times 150 \mu\text{m}^2$, and 20 kV was applied across a 4-mm gap between the specimen and the planar anode. The substrate temperature increased during the observation, and it was 159°C when the image was observed. It is clearly seen that even though the surface consists of conical structures, the specimen does not uniformly emit electrons, but there are “hot spots,” where electron emission is very intense. Assuming that the hot spots are uniformly distributed over the entire specimen surface (2 spots in a $150 \times 150 \mu\text{m}^2$ area), it follows that there were approximately 10,000 hot spots/ cm^2 . The spot size was observed by changing the FEEM magnification, but the spot size was virtually unchanged even though the magnification was maximized (the highest resolution is 20 nm). Hence, it was concluded that the hot spot size was at least smaller than 20 nm. An extrapolation of curve a of Fig. 33 to 20 kV leads to an emission current of 2.44×10^{-4} A, or 27 nA/spot on the average. It should be mentioned that, in the present FEEM setup, emitted electrons hit the anode (stainless steel), which then causes x-ray emission that irradiates the specimen. It is thus considered that the emission currents of Figs. 33(a) and 33(b) include such a secondary contribution. At the present stage, it is not quantitatively evaluated to what extent this secondary contribution is included in the total emission current.

D. Fiber formation mechanism

The present experiments on diamond films showed that both diamond etching and fiber formation occur simultaneously during the NBP treatment under conditions of {1.6 torr, -200 to -300 V, 300 to 400 W, below 700°C }, as seen in Fig. 11. By contrast, experiments under conditions of {30 torr, -300 V, 385 W, 670°C } using hydrogen plasma in the series I experiments resulted in a uniform diamond etching without fiber formation. From these results, the etching mechanism is considered to be as follows: The electron density⁶⁷ in the microwave plasma is in the order of 10^{10} – $10^{11}/\text{cm}^3$, and hence, the length of the plasma sheath⁶⁸ is evaluated to be approximately 500–1500 μm . This is much longer than the roughness of the polycrystalline diamond film surface (R_a = a few micrometers) and the powder size. Thus, hydrogen ions in the vicinity of the specimen are accelerated toward the diamond surface along a uniform electric field due to dc bias. The diamond surface reacts rapidly with incoming hydrogen ions, and the surface

carbon atoms are removed as hydrocarbon fragments and ions. Certain numbers of hydrocarbon species thus generated are redeposited on the diamond surface to form fibrous structures. This assumption is consistent with the bias-enhanced growth⁶⁹ of conelike structures of carbon under conditions of {15 torr, -180 V, 200 W, 650°C } by a microwave plasma system using 1–5 vol% CH_4/H_2 for ≤ 1 h, although the cone lengths were less than about 0.3 μm . It is inferred that the hydrocarbon fragments travel along the side surfaces of the small protuberances under the uniform electric field. By contrast, hydrogen plasma treatment of diamond without dc bias has also been investigated previously^{70–78} under various conditions, but neither fibrous nor needlelike structures were formed. These data also support the above-described mechanism of fibrous structure formation by the NBP treatment. Usually, it is oxygen but not hydrogen that has been used to etch diamond, and only uniform etching occurs.^{79–85} In Ref. 6, however, a high density of columnar structures with a diameter of 10 nm and a length of 300 nm was formed by oxygen plasma etching of a polycrystalline diamond film under a negative self bias of -300 to -400 V. The columnar structures were diamond, and not redeposited diamond nanocrystals, unlike the present results. The formation mechanism of conical structures for glasslike carbon and DLC films is considered to be the same as that of diamond. Finally, it should be emphasized that no catalyst is necessary for the formation of the fibrous structures by the NBP treatment.

IV. CONCLUSION

Diamond films and powders were treated in microwave plasma of hydrogen at 1.6 torr under a negative dc bias of around -200 V. As a result, a fibrous structure was formed on the diamond surface along the direction normal to the surface. The fiber diameter near the top end was ≤ 50 nm and the fiber lengths were ≤ 2 –3 μm . The observation by TEM indicated that the fibers consisted of diamond nanocrystals covered by amorphous layers. An overgrowth of diamond on the fibrous structure resulted in an almost uniform coating of the fibers with crystal-faceted diamond. It was also demonstrated that conical structures can be formed on glasslike carbon surface by a similar NBP treatment. It is thus envisioned more generally that fibrous structures can be formed on the surfaces of a wide range of carbon materials by the NBP treatment.

From these results, it is concluded that the formation of the fibrous structures is attributed to both the dc bias applied during the hydrogen plasma treatment and the etching chemistry at the carbon surface. It should be emphasized that the present results of fibrous structure formation are of great interest not only from a viewpoint

of plasma etching but also from a viewpoint of practical applications. So far, bulk single-crystal diamonds or CVD polycrystalline diamond films that possess flat surfaces or crystalline facets have been used for applications. However, it is likely that in many applications diamonds with fibrous surfaces will be used to achieve a practical level of performance. Finally, the present NBP treatment will be useful to modify surfaces of carbon bulk and film without metal catalyst. The fiber density and the morphology can be controlled by addition of hydrocarbon gases and oxygen to hydrogen.

ACKNOWLEDGMENTS

The authors wish to thank Dr. E. Iwamura for supplying the DLC films and Mr. K. Hayashi and Mr. M. Ohike for technical assistances. This work was carried out in the Frontier Carbon Technology (FCT) Project, which is consigned to the Japan Fine Ceramics Center (JFCC) by the New Energy and Industrial Technology Development Organization (NEDO).

REFERENCES

- R. Gomer, *Field Emission and Field Ionization* (American Institute of Physics, Woodbury, NY, 1993).
- P.K. Baumann and R.J. Nemanich, in *Low-Pressure Synthetic Diamond-Manufacturing and Applications*, edited by B. Dischler and C. Wild (Springer and Verlag, Berlin, Germany, 1998), p. 281.
- O. Gröning, O.M. Küttel, P. Gröning, and L. Schlapbach, *J. Vac. Sci. Technol. B* **17**, 1970 (1999).
- G.M. Swain, A.B. Anderson, and J.C. Angus, *MRS Bull.* **23**, 56 (1998).
- B.V. Sarada, T.N. Rao, D.A. Tryk, and A. Fujishima, *J. Electrochem. Soc.* **146**, 1469 (1999).
- H. Shiomi, *Jpn. J. Appl. Phys.* **36**, 7745 (1997).
- B.R. Stoner, G.J. Tessmer, and D.L. Dreifus, *Appl. Phys. Lett.* **62**, 1803 (1993).
- W.J. Zhang, X. Jiang, and Y.B. Xia, *J. Appl. Phys.* **82**, 1896 (1997).
- X. Jiang, W.J. Zhang, and C.P. Klages, *Phys. Rev. B* **58**, 7064 (1998).
- H. Yamamoto, K. Baba, M. Yoshimoto, and H. Takemura, in *Proceedings of the New Diamond Symposium* (New Diamond Forum, Tokyo, Japan, 1999), p. 216 (in Japanese).
- S. Iijima, *Nature (London)* **56**, 354 (1991).
- Y.S. Choi, J.H. Kang, Y.J. Park, W.B. Choi, C.J. Lee, S.H. Jo, C.G. Lee, J.H. You, J.E. Jung, N.S. Lee, and J.M. Kim, *Diamond Relat. Mater.* **10**, 1705 (2001).
- N.S. Lee, D.S. Chung, I.T. Han, J.H. Kang, Y.S. Choi, H.Y. Kim, S.H. Park, Y.W. Jin, W.K. Yi, M.J. Yun, J.E. Jung, C.J. Lee, J.H. You, S.H. Jo, C.G. Lee, and J.M. Kim, *Diamond and Relat. Mater.* **10**, 265 (2001).
- Y. Saito and S. Uemura, *Carbon* **38**, 169 (2000).
- Y. Saito, S. Uemura, and K. Hamaguchi, *Jpn. J. Appl. Phys. Part 2* **37**, L346 (1998).
- A.C. Dillon and M.J. Heben, *Appl. Phys. B* **72**, 133 (2001).
- V. Meregalli and M. Parrinello, *Appl. Phys. B* **72**, 143 (2001).
- U. Bunger and W. Zittel, *Appl. Phys. B* **72**, 147 (2001).
- T. Ishihara, A. Fukunaga, R. Akiyoshi, M. Yoshio, and Y. Takita, *Electrochemistry* **68**, 38 (2000).
- J.T. Sander, R.M. Alwin, and C.D. Verschuere, *Nature* **393**, 49 (1998).
- H.R. Shea, R. Martel, T. Hertel, T. Schmidt, and Ph. Avouris, *Microelectron. Eng.* **46**, 101 (1999).
- P.J.F. Harris, *Carbon Nanotubes and Related Structures: New Materials for the Twenty-First Century* (Cambridge Univ. Press, New York, 1999).
- Science and Application of Nanotubes (Fundamental Materials Research)*, edited by D.R. Tomanek and D. Enbody (Plenum, New York, 2000).
- O.M. Küttel, O. Gröning, C. Emmenegger, and L. Schlapbach, *Appl. Phys. Lett.* **73**, 2113 (1998).
- M. Kusunoki, T. Suzuki, K. Kaneko, and M. Ito, *Philos. Mag. Lett.* **79**, 153 (1999).
- Z.F. Ren, Z.P. Huang, J.W. Xu, J.H. Wang, P. Bush, M.P. Siegal, and P.N. Provencio, *Science* **282**, 1105 (1998).
- Z.P. Huang, J.W. Xu, Z.F. Ren, J.H. Wang, M.P. Siegal, and P.N. Provencio, *Appl. Phys. Lett.* **73**, 3845 (1998).
- K. Kobashi, T. Tachibana, Y. Yokota, N. Kawakami, K. Hayashi, and K. Inoue, *Diamond Relat. Mater.* **10**, 2039 (2001).
- K. Kobashi and T. Tachibana, *Carbon* **39**, 303 (2001).
- Handbook of Industrial Diamonds and Diamond Films*, edited by M.A. Prelas, G. Popovici, and L.K. Bigelow (Dekker, Inc., New York, 1998).
- Diamond, Electronic Properties and Applications*, edited by L.S. Pan and D.R. Kania (Kluwer Academic, Boston, MA, 1995).
- K. Kobashi, K. Nishimura, Y. Kawate, and T. Horiuchi, *Phys. Rev. B* **38**, 4067 (1988).
- S. Yugo, T. Kimura, and T. Muto, *Vacuum* **41**, 1364 (1990); S. Yugo, T. Kanai, and T. Kimura, *Diamond Relat. Mater.* **1**, 388 (1992).
- S. Yugo, T. Kanai, T. Kimura, and T. Muto, *Appl. Phys. Lett.* **58**, 1036 (1991).
- B.R. Stoner and J.T. Glass, *Appl. Phys. Lett.* **60**, 698 (1992).
- B.R. Stoner, G-H. Ma, S.D. Wolter, and J.T. Glass, *Phys. Rev. B* **45**, 11067 (1992).
- S.D. Wolter, B.R. Stoner, J.T. Glass, P.J. Ellis, D.S. Buhaenko, C.E. Jenkins, and P. Southworth, *Appl. Phys. Lett.* **62**, 1215 (1993).
- B.R. Stoner, S. Sahaida, J.P. Bade, P. Southworth, and P.J. Ellis, *J. Mater. Res.* **8**, 1334 (1993).
- T. Tachibana, K. Hayashi, and K. Kobashi, in *Advances in New Diamond Science and Technology*, edited by S. Saito, N. Fujimori, O. Fukunaga, M. Kamo, K. Kobashi, and M. Yoshikawa (MYU, Tokyo, Japan, 1994), p. 279.
- T. Tachibana, T. Hayashi, and K. Kobashi, *Appl. Phys. Lett.* **68**, 1491 (1996).
- R. Stöckel, M. Stammner, K. Janischowsky, L. Ley, M. Albrecht, and H.P. Strunk, *J. Appl. Phys.* **83**, 531 (1998).
- Y. Ando, T. Tachibana, and K. Kobashi, *Diamond Relat. Mater.* **10**, 312 (2001).
- E. Iwamura, in *Proceedings of the 2nd International Conference on Processing Materials for Properties*, edited by B. Mishra and C. Yamauchi (The Minerals, Metals & Materials Soc., Warrendale, PA, 2000), p. 263; B. Window and G. L. Harding, *J. Vac. Sci. Technol. A* **8**, 1277 (1990).
- Y. Gotoh, T. Kondo, M. Nagao, H. Tsuji, J. Ishikawa, K. Hayashi, and K. Kobashi, *J. Vac. Sci. Technol. B* **18**, 1018 (2000).
- R.J. Nemanich, S.L. English, J.D. Hartman, A.T. Sowers, B.L. Ward, H. Ade, and R.F. Davis, *Appl. Surf. Sci.* **146**, 287 (1999).
- J.D. Hartman, K. Naniwae, C. Petrich, V. Ramachandran, R.M. Feenstra, R.J. Nemanich, and R.F. Davis, *Mater. Sci. Forum* **338(I)**, 353 (2000).

47. F.A.M. Köck, J.M. Garguilo, B. Brown, and R.J. Nemanich, in *Electron-Emission Materials, Vacuum Microelectronics and Flat-Panel Displays*, edited by K.L. Jensen, R.J. Nemanich, P. Holloway, T. Trottier, W. Mackie, D. Temple, and J. Hoh (Mater. Res. Soc. Symp. Proc. **621**, Warrendale, PA, 2000), p. R651
48. K.M. Rutledge and K.K. Gleason, in *Handbook of Industrial Diamonds and Diamond Films*, edited by M.A. Prelas, G. Popovici, and L.K. Bigelow (Dekker, Inc., New York, 1998), Chap. 9, p. 413.
49. L.S.G. Plano, in *Diamond, Electronic Properties and Applications*, edited by L.S. Pan and D.R. Kania (Kluwer Academic, Boston, MA, 1995), Chap. 3, p. 61.
50. W. Zhang, F. Zhang, Q. Wu, and G. Chen, *Mater. Lett.* **15**, 292 (1992).
51. K.M. McNamara, B.E. Williams, K.K. Gleason, and B.E. Scraggs, *J. Appl. Phys.* **76**, 2466 (1994).
52. B. Dischler, C. Wild, W. Muller-Sebert, and P. Koidl, *Physica B* **185**, 217 (1993).
53. K. Hayashi, S. Yamanaka, H. Okushi, and K. Kajimura, *Diamond Relat. Mater.* **5**, 1002 (1996).
54. H. Kawarada, *Surf. Sci. Rep.* **26**, 205 (1996).
55. K. Hayashi, S. Yamanaka, H. Okushi, and K. Kajimura, *Appl. Phys. Lett.* **68**, 376 (1996).
56. Y. Mori, E. Mori, A. Hatta, T. Ito, and A. Hiraki, *Jpn. J. Appl. Phys. Part 2* **31**, L1720 (1992).
57. M.I. Landstrass and K.V. Ravi, *Appl. Phys. Lett.* **55**, 975 (1989); *Appl. Phys. Lett.* **55**, 1391 (1989).
58. S.A. Grot, G.S. Gildenblat, C.W. Hatfield, C.R. Wronski, A.R. Badzian, T. Badzian, and R. Messier, *IEEE Electron Device Lett.* **11**, 100 (1990).
59. T. Maki, S. Shikama, M. Komori, Y. Sakaguchi, K. Sakuta, and T. Kobayashi, *Jpn. J. Appl. Phys. Part 2* **31**, L1446 (1992).
60. Y. Mori, Y. Show, M. Deguchi, H. Yagi, H. Yagyu, N. Eimori, T. Okada, A. Hatta, K. Nishinura, M. Kitabatake, T. Ito, T. Hirao, T. Izumi, T. Sasaki, and A. Hiraki, *Jpn. J. Appl. Phys.* **32**, L987 (1993).
61. S. Albin and L. Watkins, *Appl. Phys. Lett.* **56**, 1454 (1990).
62. K. Hayashi, S. Yamanaka, H. Watanabe, T. Sekiguchi, H. Okushi, and K. Kajimura, *J. Appl. Phys.* **81**, 744 (1997).
63. R.J. Nemanich, L. Bergman, Y.M. LeGrice, K.F. Turner, and T.P. Humphreys, *Proc. SPIE* **1437**, 2 (1991).
64. Y. Ando, Y. Nishibayashi, and K. Kobashi, *Diamond Relat. Mater.* **10**, 606 (2001).
65. A.T. Sowers, B.L. Ward, S.L. English, and R.J. Nemanich, *J. Appl. Phys.* **86**, 3973 (1999).
66. Q. Chen and G.M. Swain, *Langmuir* **14**, 7017 (1998).
67. A. Gicquel, in *Handbook of Industrial Diamonds and Diamond Films*, edited by M.A. Prelas, G. Popovici, and L.K. Bigelow (Dekker, New York, 1998), p. 583.
68. M.A. Lieberman and A.J. Lichtenberg, *Principles of Plasma Discharges and Materials Processing* (Wiley, New York, 1994).
69. Y-T. Trong, H-C. Hsieh, and C-F. Chen, *Diamond Relat. Mater.* **8**, 772 (1999).
70. O.M. Küttel, L. Diederich, E. Schaller, O. Carnal, and L. Schlapbach, *Surf. Sci.* **337**, L812 (1995).
71. R.E. Rawles, S.F. Komarov, R. Gat, W.G. Morris, J.B. Hudson, and M.P. D'Evelyn, *Diamond Relat. Mater.* **6**, 791 (1997).
72. C-L. Cheng, H-C. Chang, J-C. Lin, K-J. Song, and J-K. Wang, *Phys. Rev. Lett.* **78**, 3713 (1997).
73. T.W. Mercer, J.N. Russel, Jr., and P.E. Pehrsson, *Surf. Sci.* **392**, L21 (1997).
74. K. Hayashi, S. Yamanaka, H. Ohkushi, and K. Kajimura, *Diamond Relat. Mater.* **5**, 1002 (1996).
75. K. Hayashi, S. Yamanaka, H. Watanabe, T. Sekiguchi, H. Ohkushi, and K. Kajimura, *Appl. Surf. Sci.* **125**, 120 (1998).
76. B. Koslowski, S. Strobel, M.J. Wenig, and P. Ziemann, *Appl. Phys. A* **66**, S1159 (1998).
77. B. Koslowski, S. Strobel, M.J. Wenig, R. Martschat, and P. Ziemann, *Diamond Relat. Mater.* **7**, 322 (1998).
78. Y.P. Guo, K.L. Lam, K.M. Lui, R.W.M. Kwok, and K.C. Hui, *J. Mater. Res.* **13**, 2315 (1998).
79. C. Hata, M. Kamo, and Y. Sato, *New Diamond* (MYU, Tokyo, 1989), No. 5, p. 12 (in Japanese).
80. N. Uchida, T. Kurita, K. Uematsu, and K. Saito, *J. Mater. Sci. Lett.* **9**, 249 (1990); N. Uchida, T. Kurita, H. Ohkushi, K. Uematsu, and K. Saito, *J. Cryst. Growth* **114**, 565 (1991).
81. C.J. Chu, C. Pan, J.L. Margrave, and R.H. Hauge, *Diamond Relat. Mater.* **4**, 1317 (1995).
82. J. Taniguchi, I. Miyamoto, N. Ohno, and S. Honda, *Jpn. J. Appl. Phys.* **35**, 6574 (1996); S. Kiyohara and I. Miyamoto, *Nanotechnology* **7**, 270 (1996).
83. S. Kiyoyama, I. Miyamoto, K. Kitazawa, and S. Honda, *Nucl. Instrum. Methods Phys. Res. Sect. B* **121**, 510 (1997).
84. R. Ramesham and B.H. Loo, *J. Electrochem. Soc.* **139**, 1988 (1992).
85. R. Ramesham, W. Welch, W.C. Neely, M.F. Rose, and R.F. Askew, *Thin Solid Films* **304**, 245 (1997).